Propagating Interictal Spikes in the neocortex: Relationship to Inactivated Action Potentials, and implications for Epileptogenesis

by

Crispin Foli

A Thesis Presented in Partial Fulfillment
of the Requirements for the Degree
Master of Science

Approved April 2021 by the
Graduate Supervisory Committee:

Bradley Greger, Chair
Jitendran Muthuswamy
Konstantinos Tsakalis

ARIZONA STATE UNIVERSITY

May 2021

ABSTRACT

Interictal spikes - transient bursts of neuronal depolarization observed between epileptic seizures - are typically regarded as a sign of epilepsy and have been used in the localization of seizure onsets. Interictal spikes are thought to arise primarily from large excitatory postsynaptic potentials (EPSPs), although not much is known about the precise role they play in epilepsy. Here the *in vivo* spatiotemporal dynamics of sequences of interictal spikes in a small (4mm x 4mm) patch of the cortex of a patient with intractable epilepsy is studied. In conjunction with this, the impact on action potential generation and firing of local voltage changes due to paroxysmal depolarizations similar to interictal spikes was also evaluated *in vitro* using resected neural tissue from an epileptic human neocortex. Sequences of interictal spikes were found to consistently propagate in a direction-specific manner across the neocortex. In addition to this, bursts of action potentials from the *ex vivo* samples underwent variable degrees of depolarization-induced inactivation. Intracellular recordings in neocortical slices of human brain tissue confirmed that bursts of inactivated action potentials occurred during spontaneous paroxysmal depolarization shifts. These *ex vivo* findings showed inactivated action potentials being generated by large depolarizations. The results suggest the existence of an aberrantly strong synchronization among neuronal populations in the epileptic cortex, triggered or enhanced by interictal spike depolarization and propagation. This supports a key element in the hypothesis that interictal spikes, and the associated alteration of action

potential firing patterns, may alter the electrical environment of the brain and contribute to the progression of the underlying idiopathic seizure disorder.

DEDICATION

This work is dedicated to all family and friends for their support, prayers, and well-wishes.

ACKNOWLEDGMENTS

The author would like to express profound appreciation to Drs. Bradley Greger, Jitendran Muthuswamy and Konstantinos Tsakalis for their invaluable support and guidance to the completion of this work.

TABLE OF CONTENTS

Page

Page

LIST OF TABLES

LIST OF FIGURES

INTRODUCTION

About one-third of patients with idiopathic seizure disorder have seizures that cannot be controlled by medication [1]. The limited treatment options available to such patients include surgical resection of the epileptogenic zone (the region of cortex where seizures are initiated), and/or the use of devices to reduce seizure frequency [2]. Each of these methods relies on the utility of electrographic discharges between (interictal) and during (ictal) seizures to predict seizures [3] and to localize the epileptogenic zone [2], [4]–[7]. In the interictal recordings, the main paroxysmal events of clinical significance are the interictal spikes. Interictal spikes are brief [8] abnormal depolarizations of groups of neurons that occur between seizures and arise from the simultaneous firing of hyperexcitable neurons [9]–[12]. These paroxysmal discharges are clearly distinguishable from background activity, usually with a negative-going peak and an abrupt change in polarity lasting several milliseconds [13]. Given their relative abundance in recordings of electrographic events in epilepsy, interictal spikes comprise a more attractive target for treating intractable epilepsy [14]. The efficacy of their utility depends on an accurate understanding of their role and contribution to epilepsy. Interictal spikes are typically designated as important biomarkers of epilepsy [15], [16], and are hypothesized to be indicative of an underlying pathologic cellular synchronization [17]. However, their precise relationship and the implications of their presence to seizures as well as their correlation with epileptogenesis is poorly understood [18]–[20]. Multiple studies have

investigated changes in interictal spike patterns before seizures as a means of identifying their relationship to seizures in epilepsy [2], [19], [21]. It has been suggested that abnormal networks in epilepsy are not limited to periods of seizures only, but could also be strongly influenced by interictal spike patterns [22], [20]. Other studies have explored the role of interictal spikes in planning surgical resection [19], [23], [24], [25], though their utility is disputed because they are thought to propagate out of the epileptogenic zone [19], [26], [27].

Here the spatial dynamics in interictal spikes over time, as well as the physiological mechanisms underlying interictal spike depolarization is studied. Using a combination of *in vivo* intracortical and *ex vivo* intracellular methods, this study investigated i) spatiotemporal dynamics observed in interictal spike sequences to map out their propagation patterns (propagation direction and speed), and ii) the use of intracellular recordings to analyze changes in single unit activity due to paroxysmal depolarization. Using recordings from a slice of the epileptic human cortex, the effects of depolarization on action potential firing patterns in a patient with idiopathic seizure disorder is studied. Specifically, the intracellular studies evaluate how the depolarization of neuronal membranes leads to increased inactivation of sodium channels and causes action potential waveform durations to increase and waveform amplitudes to decrease. This phenomenon of depolarization-induced inactivation of action potentials also occurs in mammalian pyramidal cells [28], [29]. The goal was to understand how interictal spike depolarization affected action potential inactivation in neurons and the implication of that to the progression of the disease. Studying

alterations to cellular activity and neuronal firing patterns due to interictal spike depolarization, as well as mapping out the propagation patterns of these depolarizations allows us to better evaluate the relationship between these physiological phenomena observed in epilepsy. The presence of depolarization-induced bursts of normal and inactivated action potentials coupled with the temporal propagation of these depolarization currents in the neocortex may have significant implications for the pathogenesis of idiopathic seizure disorders.

MATERIALS AND METHODS

Electrode array implantation

This study was approved by the Institutional Review Boards at all institutions including Arizona State University, the University of Utah, and Columbia University, and informed consent was obtained from the patient with idiopathic seizure disorder. One patient underwent surgical placement of electrocorticography grids for the localization of epileptic foci prior to surgical resection. The patient was also implanted with a single microelectrode array (Blackrock Microsystems, SLC, UT) [30] (Table 1) (figure 1).

The microelectrode array used in this study was the FDA-approved NeuroPort Array that has been safely implanted in humans at several institutions [30]–[32] and for over 1000 days [33]. The array measures 4 x 4 mm and contains 96 microelectrodes arranged in a regular 10 x 10 square. The individual microelectrodes were platinum-coated

silicon, protruding 1 mm from the array base and were electrically insulated except for the terminal 70 µm. They tapered from 35–75 µm in diameter at the base to 3–5 µm at their recording tips. The mean electrode impedances at 1 kHz on the microelectrode arrays before implantation was: 311±154 kΩ.

Patient	Age	Gender	Epileptogenic zone	UEA implant site	Pathology	Outcome
1	30	Male	Right lateral and mesial temporal lobe; nonlesional	Right middle temporal gyrus, 4 cm posterior to the temporal pole	Mesial temporal sclerosis	Engel 2 at 22 months

Table 1. Patient information and outcome.

The patient in this study was a 30-year-old male undergoing presurgical evaluation. The patient was implanted with both ECoG grid and microelectrode array, but this study is limited to the microelectrode array recording. The microelectrode array was implanted in the right middle temporal gyrus of the patient, who had been diagnosed with mesial temporal sclerosis.

In vivo recording

Broadband (0.3–7500 Hz, 30 kHz sampling rate) neural data from the microelectrode array were recorded using a Neuroport System (Blackrock Microsystems) (Figure 1). The microelectrode array was implanted in the area targeted for subsequent surgical removal. The microelectrode array was implanted into a flat surface of exposed neocortical gyrus through the pia mater using a pneumatic insertion technique using previously described

methods [31], [32], [34]. The microelectrode array assembly includes two reference wires. After the monitoring period, with duration determined by clinical needs, the microelectrode array was explanted. The location of the microelectrode array was co-registered to the cortical anatomy using preoperative magnetic resonance imaging studies and postoperative computed tomography scans [35].

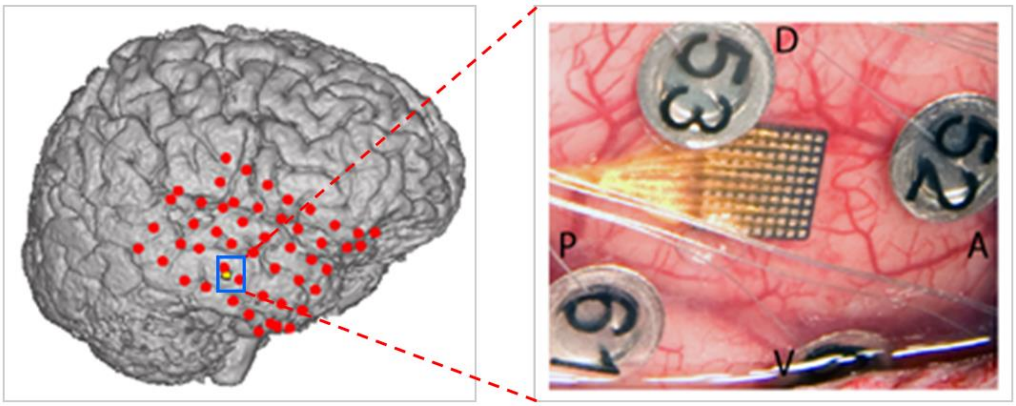

Figure 1. Implanted microelectrode array.

The microelectrode array was implanted in the right middle temporal gyrus in the Patient. The locations of the microelectrode array (yellow square) and ECoG grid electrodes (red circles) from the post-operative CT were co-registered with the preoperative magnetic resonance imaging. The intraoperative photograph shows the microelectrode array and nearby ECoG electrodes with the same orientation as in the magnetic resonance imaging (A = anterior, P = posterior, D = dorsal, V = ventral)

Identification of interictal spikes

The dynamics in synchronization and excitation among neurons in the epileptic cortex manifest as interictal spikes of various shapes and forms [36] (Figure 2). Generally, interictal spikes recorded in epilepsy are periodic high-amplitude events lasting between 20ms and 250ms. Interictal spikes include short duration transients known as spikes (< 50ms), as well as slower electrographic discharges known as sharp waves (50ms to 200ms) [37]–[39]. During interictal recordings, multiple variants of interictal spikes are often observed spatiotemporally. For this project, however, these variants of interictal spikes are not differentiated, since they have been reported to be merely morphological, with no significant clinical reason for differentiation [13]. Prior to identifying interictal spikes, the broadband (0.3–7500 Hz, 30 kHz sampling rate) neural data from the microelectrode array were bandpass filtered (passband frequency of [1-50Hz]) to extract local field potentials of interest. Interictal spikes typically have a frequency band of <20Hz [13]. Characteristic kinetic features were used to identify interictal spikes from the recorded microelectrode field potentials. For each channel, thresholding was used to identify potential interictal spike waveforms of interest as follows: All threshold crossings of interest met at least one of two criteria: (i) a negative peak amplitude crossing below three times the standard deviation of that recorded channel, (ii) a minimum negative peak prominence of at least a third of the standard deviation of that recorded channel. Threshold crossings occurring within 200ms of an initially detected threshold crossing were automatically discarded. A 200ms window centered around the

timestamp corresponding to each detected threshold crossings was used to extract candidate interictal spike waveforms. The waveforms identified this way were then visually evaluated to exclude artefactual waveforms. This allowed for all apparent algorithmic deficiencies to be corrected for and clearly defined interictal spike waveforms recorded simultaneously across all electrodes to be identified. Since the detection algorithm also automatically detected the time of the negative peak of detected interictal spikes, the visual evaluation also allowed for selecting only those interictal spikes with clearly defined and detected negative peaks to be selected. This was to ensure uniformity and accuracy of the measure of the relative timing of interictal spikes across all electrodes. The resulting waveforms were classified into interictal spike sequences. An interictal spike sequence consisted of 96 interictal spikes simultaneously recorded by the 96 electrodes in the microelectrode array within the same 200ms period. For example, for an interictal spike occurring at time t, a window defined from $[-100ms\ to\ 100ms]$, centered around t was used to index into all channels to extract the interictal spike waveform recorded by that electrode within this window. The time of the negative peak of the waveforms detected by each electrode is designated as the time the interictal spike hit that electrode. This relative timing of interictal spikes detected by all electrodes within the same 200ms window was later used to map out interictal spike propagation directions.

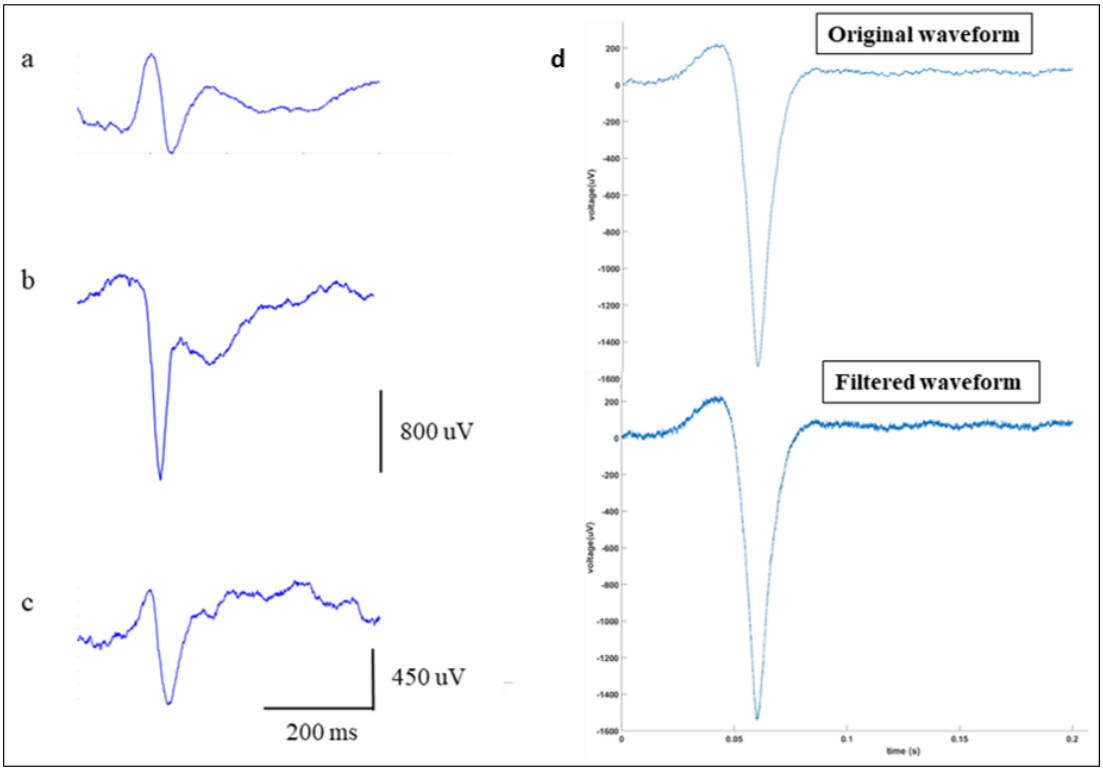

Figure 2. Interictal spike variants

Dynamic changes in synchronization and excitation among neurons give rise to interictal spikes of various morphologies. These range from short duration and high amplitude spikes (typically <50ms) to much slower sharp waves (typically between 50ms and 200ms). Figure 2 a, b, and c show sample interictal spikes recorded in the patient at different time instants on different electrodes. Interictal spikes with different kinetics are often recorded from around the same cortical region over time. These, however, have been identified to have no distinctive physiologic characteristics of interest in clinical applications. This study does not decompose interictal spikes into subtypes based on kinetics. Figure 2 d shows a filtered vs an unfiltered interictal spike waveform.

Interictal spike propagation

The time at which the negative peak of the interictal spike waveform occurred was determined for each electrode across the microelectrode array. If the interictal spikes travelled in a coherent direction, the negative peak of the propagating wave would reach electrodes along this axis sequentially in time. For each sequence of interictal spikes detected within the same 200ms time segment by all electrodes, clear latencies in the timing of negative peaks were observed (figure 3). A "latency" map was created for each interictal spike sequence. This map was based on the geometric layout of the microelectrode array and highlighted the relative times of interictal spikes detected on all electrodes, using color codes for easy visualization and further analysis.

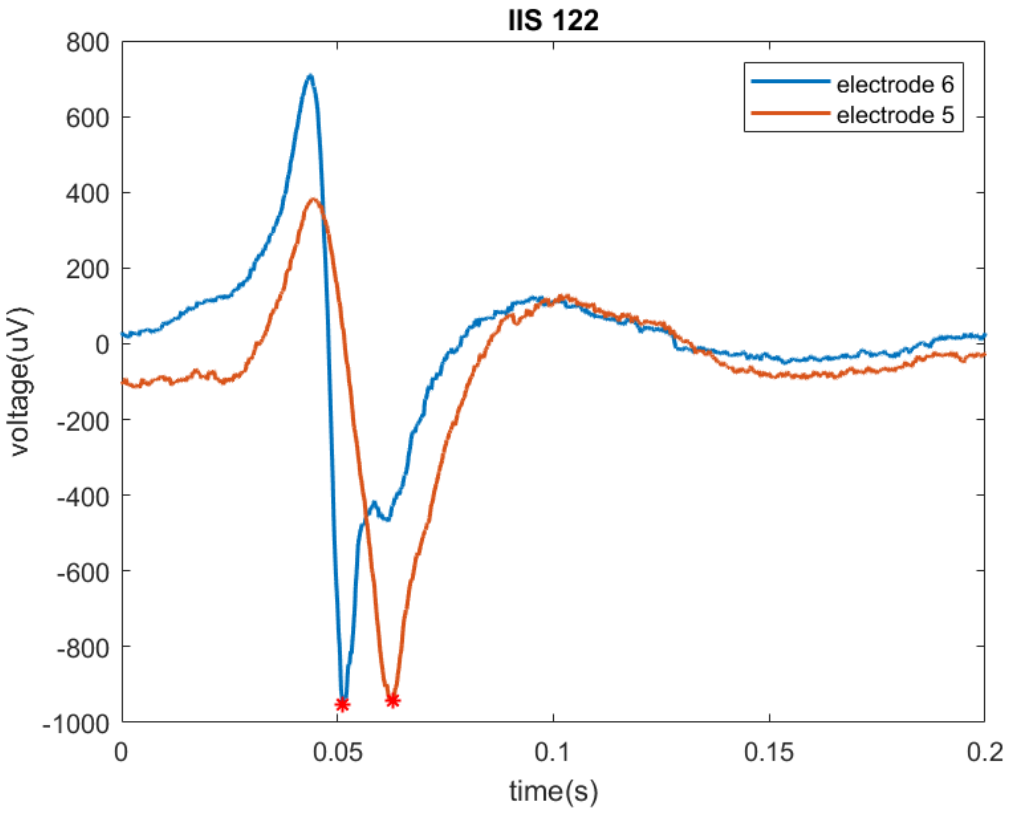

Figure 3. Observed latencies between interictal spikes on different electrodes.

Figure 3 shows the 122nd interictal spike on electrode 5 and 6, highlighting the temporal delays observed between them. Interictal spikes recorded within the same 200ms time instant across all electrodes showed clear delays in the relative timing of their negative peaks. The timing of the negative peak of the interictal spike on each electrode was used as a measure of when the interictal spike hit that electrode, relative to the neighboring electrodes. This latency in negative peak times was used to map out the propagation pathway of interictal spikes across the microelectrode array.

To map out the trajectory of interictal spikes across the entire array for each sequence of interictal spikes, directional gradients among neighboring electrodes were calculated using the relative timing of the negative peaks of interictal spikes recorded by all electrodes. The directional gradient algorithm mapped out the directions of maximal increase between electrodes, using the interictal spike negative peak times. For example, for interictal spike K on electrode N, the algorithm takes into consideration the timing of the negative peaks of the corresponding (Kth) interictal spike on the neighboring electrodes of electrode N and returns a single vector pointing in the direction of maximal time difference. This gradient vector highlights the local propagation direction, from electrode N. In other words, it predicts the propagation path of the interictal spike K from electrode N. This process was repeated for all electrodes to give multiple gradient vectors corresponding to all the electrodes in the array. The average of these vectors gave a single gradient vector corresponding to the average propagation direction of the current interictal spike across the entire microelectrode array. The average of the negative peak times of interictal spikes at the middle four electrodes was designated as the origin (time zero). The magnitude (radius) of the gradient vector determined this was also predicted the speed of propagation across the microelectrode array. Thus, for each interictal spike, the direction of the gradient vector predicted the propagation direction of that interictal spike across the entire array, while its radius predicted the speed of propagation.

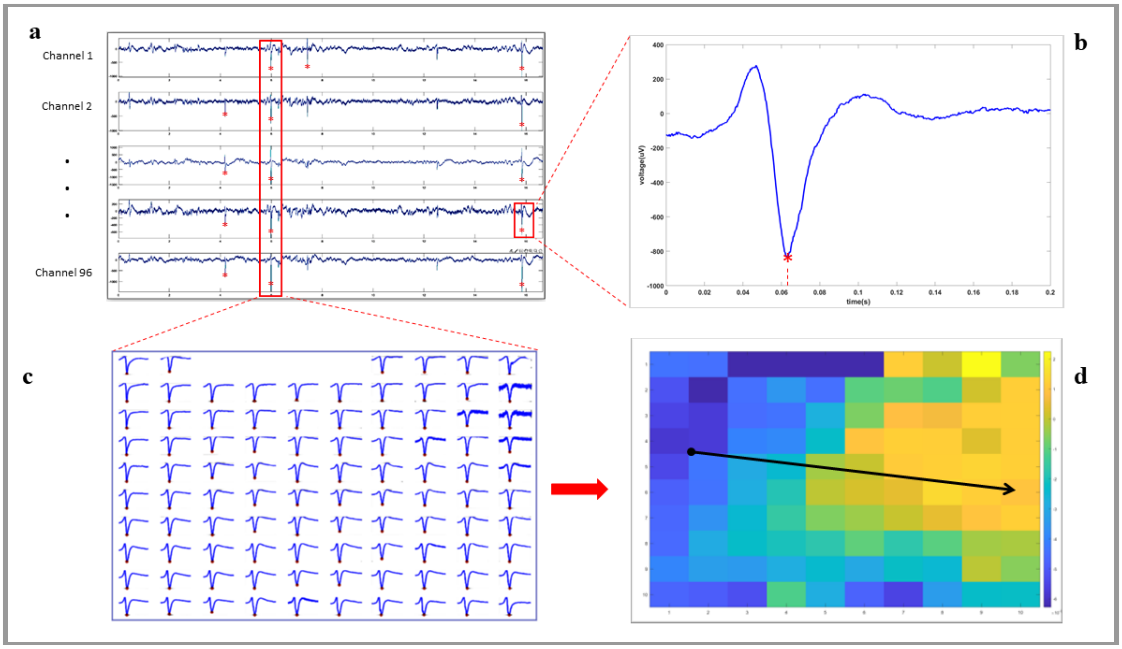

Figure 4. Interictal spike identification and propagation.

a) Recordings of interictal events in epilepsy showed brief paroxysmal depolarizations identified to be interictal spikes. These were clearly distinguishable from the background activity, allowing for extraction through thresholding. Sequences of interictal spikes occurring within the same time segment on all electrodes are identified using a windowing method discussed above. b) Interictal spikes arise from synchronized depolarization of hyperexcitable neuronal ensembles within the epileptic network. These waveforms typically last between 20ms and 200ms. c) The time of the negative peaks of interictal spikes occurring within the same 200ms time window were identified. d) Using the identified negative peak times, and the geometric layout of the microelectrode array, a latency map highlighting propagation delays was constructed. From this, the propagation speed and direction of interictal spikes across the microelectrode array were estimated by calculating directional gradients.

Ex vivo recording

A small block of brain tissue adjacent to the microelectrode array was surgically removed and placed in a partially frozen oxygenated slicing solution (saturated with 95% oxygen, 5% carbon dioxide) containing (in mM): 220 sucrose, 3 KCl, 10 $MgSO_4$, 1.25 NaH_2PO_4, 25 $NaHCO_3$, 25 D-glucose, and 0.2 $CaCl_2$. Neocortical slices were cut at a thickness of 450 mm with a vibratome (Lancer series 1000, St. Louis, MO). Slices were then transferred into an artificial cerebrospinal fluid-containing (in mM): 124 NaCl, 3 KCl, 26 $NaHCO_3$, 1.4 NaH_2PO_4, 2 $CaCl_2$, 2 $MgSO_4$, and 11 glucose, and were allowed to recover for 32 hours in a submerged storage chamber maintained at 32–34°C before they were mounted onto a ramp-type interface chamber for electrophysiological recording. Nine neurons were recorded from a single brain slice. Of those nine neurons, four were analyzed due to the fact that strong depolarizations generated a large number of action potentials.

Simultaneous extracellular field-potential and whole-cell patch-clamp recordings were done in layer II/III of the neocortex with an Axoprobe-1A amplifier and an Axopatch-1D amplifier (Axon Instruments, Foster City, CA), respectively. Extracellular recordings were DC-coupled. Electrodes were placed ~100 μm apart. During recording, the extracellular [K+] in aCSF was elevated to 8–11 mM to induce epileptiform bursts [40]. Since interictal spikes do not occur in excised tissue with normal artificial cerebrospinal fluid, action potentials generated during spontaneously occurring paroxysmal

depolarization shifts were examined. All signals were sampled at 10 kHz, low-pass filtered at 2 kHz, and recorded with pClamp 8.0 (Molecular Device, Union City, CA) through a Digidata-1320A digitizer (Clampex, Molecular Device).

Thick-wall glass pipettes with a tip of 1–3 mm were used for both extracellular and whole-cell recordings and were pulled from borosilicate glass capillaries (OD 1.65 mm, ID 1.2 mm, Garner Glass, Claremont, CA) with a P-87 Flaming-Brown puller (Sutter Instruments, Novato, CA). For extracellular recordings, pipettes were filled with artificial cerebrospinal fluid. For whole-cell recordings, pipettes were filled with intracellular solution containing (in mM): 130 K-gluconate, 2 NaCl, 2 KCl, 1 $MgCl_2$, 0.5 $CaCl_2$, 5.5 EGTA, 10 HEPES, 10 phosphocreatine-tris, 0.5 NaGTP, and 4 MgATP. The pH was adjusted to 7.2 with 5 M KOH. Patch pipettes had a resistance of 5–7 MW when filled with this solution.

Each of the action potential peaks was found by setting parameters. A minimum prominence threshold, a minimum separation value, an interictal spike threshold for normal action potentials, and an interictal spike threshold for inactivated action potentials for each of the nine neurons can be seen in Table 2:

Neuron #	Minimum Prominence Threshold	Minimum Separation	Interictal Spike Threshold for Normal APs	Interictal Spike Threshold for Inactivated APs
1	30 mA	0.100 ms	< -35 mA	> -33 mA
2	30 mA	0.100 ms	< -40 mA	> -35 mA
3	30 mA	0.100 ms	< -35 mA	> -26 mA
4	30 mA	0.100 ms	< -35 mA	> -26 mA
5	30 mA	0.100 ms	< -35 mA	> -26 mA
6	30 mA	0.100 ms	< -35 mA	> -26 mA
7	30 mA	0.100 ms	< -35 mA	> -26 mA
8	30 mA	0.100 ms	< -35 mA	> -26 mA
9	30 mA	0.100 ms	< -35 mA	> -26 mA

Table 2. Activation thresholds for neurons

Different thresholds were set for each of the neurons to identify action potentials as well as inactivated action potentials.

RESULTS

Propagation of interictal spike sequences

Observation of the voltages on all electrodes in the array over time during interictal spikes showed that interictal spikes propagated across the microelectrode array. The time of the negative peaks of interictal spikes on each electrode in the array were calculated. Because of the fixed geometry of the microelectrode array, it was possible to use the difference in the time the negative peak arrived at each electrode to quantify the direction and speed of interictal spike propagation. Interictal spikes were found to consistently propagate across the array over time. The average direction of propagation was consistent to within a few tens of degrees. Of all the 200 interictal spikes studied, the mean and median propagation directions, as calculated using directional gradients, were 29° and 28° respectively (0° = anterior, 90° = dorsal, 180° = posterior, 270° = ventral). The

propagation directions for all interictal spikes showed a bell-shaped distribution (Figure 6), with a standard deviation of 42°. Analyzing interictal spike propagation direction over time revealed there was no significant correlation between time and propagation direction (figure). However, majority (72%) of interictal spikes propagated within one standard deviation of the mean propagation direction. Interictal spike propagation speeds were found by computing the radius of the propagation vectors. Propagation speeds ranged from 0.21m/s to 2.77m/s, with a mean speed of 1.34m/s. The histogram of propagation speeds for all interictal spikes also showed a bell-shaped (figure). Propagation speeds did not deviate significantly or correlate with time. More than 60% of all propagation speeds were within one standard deviation of the mean propagation speed (1.34m/s).

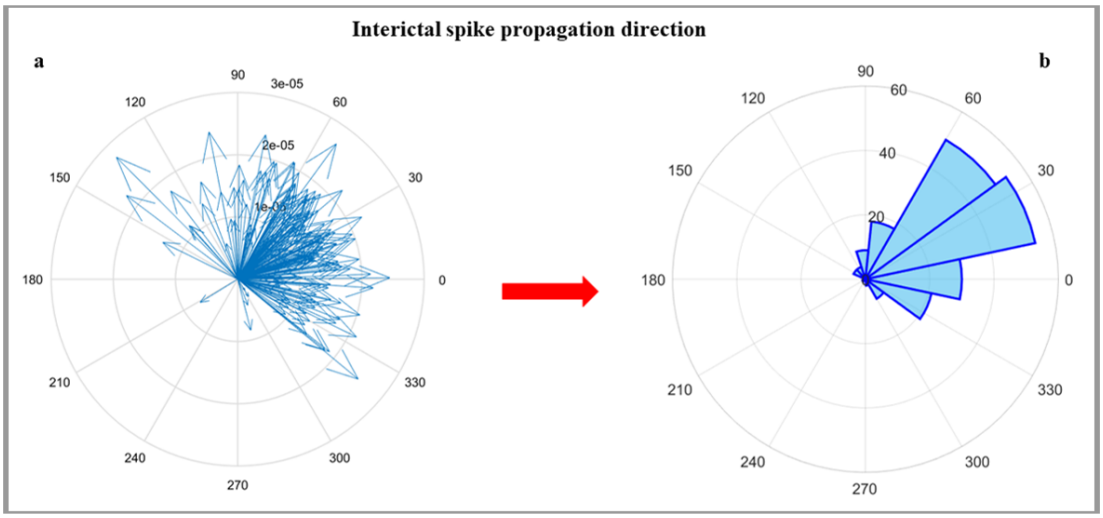

Figure 5. Interictal spike propagation over time.

a) A collection of all propagation vectors for all interictal spikes analyzed are shown. Each arrow (vector) represents an interictal spike: the direction of the arrow shows the propagation direction of that interictal spike, while the length (radius) of the vector corresponds with the propagation speed. The propagation direction of each interictal spike recorded on the microelectrode arrays was calculated using the methods described above. Interictal spikes propagated consistently in a direction-specific manner across the microelectrode array over time, with minimal deviation from the mean propagation direction. Since the propagation direction was estimated using the times of the negative peaks of interictal spikes on all electrodes, the average negative peak time of the middle four electrodes was used as the reference point (time zero). b) The distributions of propagation directions are displayed as angular histograms. This highlights the number of interictal spikes propagating in each range of directions, specified in degrees. (0° = anterior, 90° = dorsal, 180° = posterior, 270° = ventral).

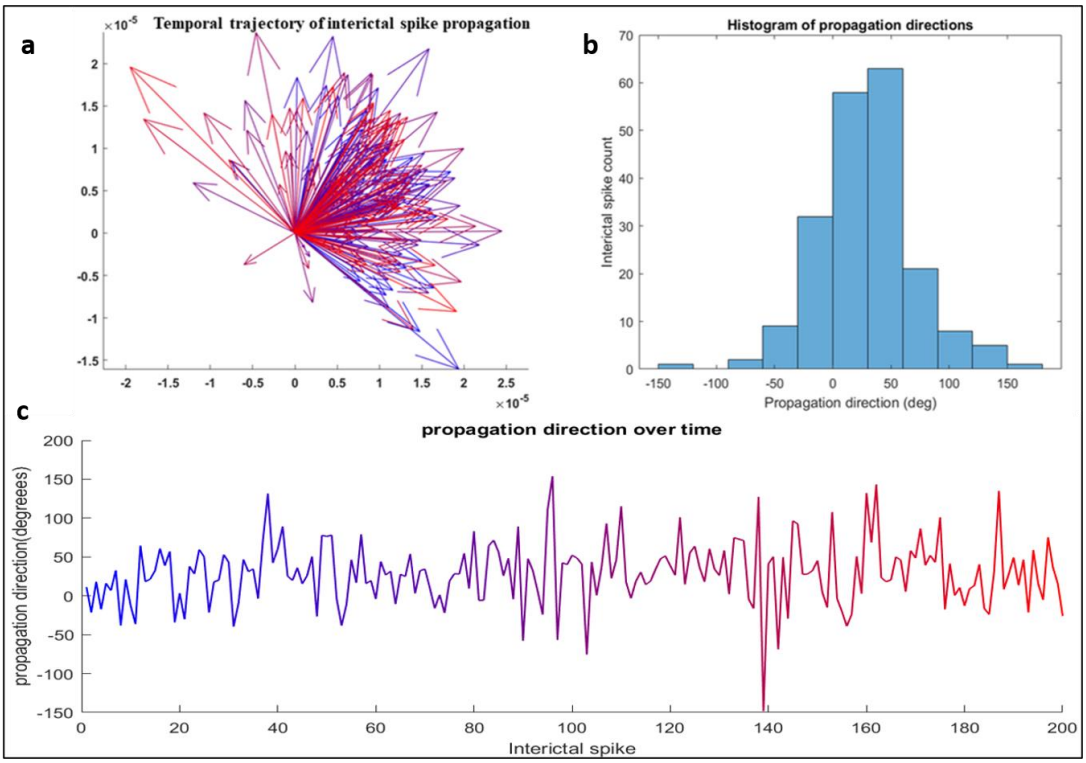

Figure 6. Temporal variation in propagation direction.

a) Interictal spike propagation directions were aligned with their occurrence times, to access the relationship between interictal spike occurrence times and propagation direction. The color codes highlight interictal spike timing for better visualization: blue arrows correspond to early interictal spikes, while red ones depict interictal spikes that occurred later in the interictal recording. Overall, no correlation between interictal spike occurrence time and propagation direction was identified. b) The distribution of interictal spike propagation direction is shown. This depicts a normal distribution, with a mean propagation direction of 29° (0° = anterior, 90° = dorsal, 180° = posterior, 270° = ventral). Approximately 72% of interictal spikes propagated within one standard deviation of the mean propagation direction, highlighting the consistency observed in propagation direction over time. Figure 6 c) also shows propagation direction over time, as a time series plot.

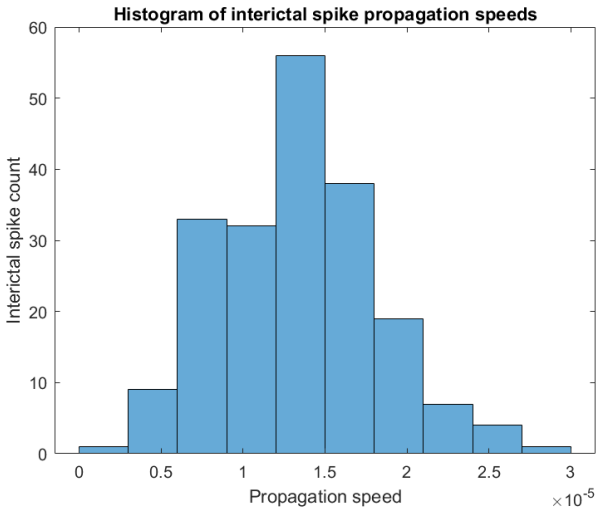

Figure 7. Interictal spike propagation speeds.

The propagation speeds of all interictal spikes analyzed showed little variation over time. The propagation speeds ranged from 0.21m/s to 2.77m/s, with a mean speed of 1.34m/s. More than 60% of all propagation speeds were within one standard deviation of the mean propagation speed (1.34m/s).

Interictal spike amplitude distributions in the microelectrode array

In addition to studying the topographical propagation of interictal spikes across the cortex, laminar dynamics where also assessed using the amplitudes of the negative peaks of interictal spikes. The microelectrode array was implanted onto the right middle temporal gyrus of the patient. Given the fixed geometry of the microelectrode array and the curviform anatomy of the gyrus, the goal of this analysis was to investigate depth-wise spatial dynamics in interictal spike patterns across the cortex. Similar studies of

laminar dynamics in animal models have reported “vertical” propagations of interictal events [41]–[45]. One of those studies [45], which recorded and analyzed interictal spike potentials at different cortical layers in cat striate cortical neurons, reported finding systematic changes in interictal spike amplitudes at varying depths in the cortex. From the findings, it was proposed that different cortical layers possibly have different levels of contribution to epileptogenesis. A similar observation of depth-dependent interictal spike amplitude levels was made in this study of interictal spikes in human epileptic cortex. As with the negative peak times, the negative peak voltage of interictal spikes on all electrodes were mapped onto the geometric layout of the microelectrode array. These were color-coded to emphasize the relative magnitudes of interictal spikes at different electrode sites (Figure 8). The negative peak amplitudes were found to show a stereotyped distribution, suggesting the presence of depth-dependent amplitude dynamics. The middle electrodes recorded the highest interictal spike amplitudes. These amplitudes decreased toward the edges of the microelectrode array. This distribution of amplitudes was observed consistently for all interictal spikes analyzed. Figure 8 shows the average of these amplitude distributions.

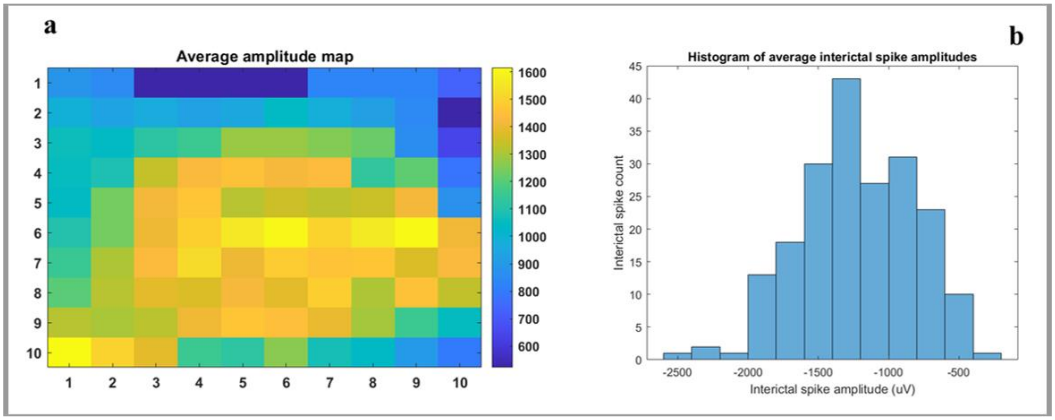

Figure 8. Average interictal spike amplitude distribution.

a) The amplitudes of interictal spikes across the microelectrode array consistently showed a characteristic distribution pattern suggestive of depth modulation of interictal spike amplitudes. Figure 8a shows the average of this distribution for all interictal spikes over time. b) The average amplitude across the entire microelectrode array for all interictal spike sequences was calculated, giving rise to 200 "average" interictal spike amplitudes. The histogram shows the distribution of average amplitudes over time.

Paroxysmal depolarization and action potential inactivation in vitro

To examine the impact of interictal spikes on the waveforms of action potentials, *in vitro* simultaneous intracellular and extracellular recordings were performed on nine neurons in cortical tissue resected from adjacent to the microelectrode array in the patient. Interictal spikes have been studied in both *in vivo* animal models and *in vitro* brain slices from animals and humans using large paroxysmal depolarization shifts as a model of interictal

spikes [46]–[50]. Since interictal spikes do not occur in excised tissue with normal artificial cerebrospinal fluid (aCSF), action potentials generated during spontaneously occurring paroxysmal depolarization shifts when the potassium concentration in the aCSF was elevated to 8–11 mM were examined. Intracellularly recorded bursts of action potentials were observed during extracellularly recorded paroxysmal depolarization shifts. These action potentials exhibited broad, longer-duration waveforms (i.e., longer wavelength) with a reduced amplitude that are characteristic of inactivated action potentials [29], [50], [51], which resulted in a shift in the spectral power to lower frequencies. Nine neurons were recorded from a single patient. The action potentials recorded in the first neuron are shown in figure 7 below:

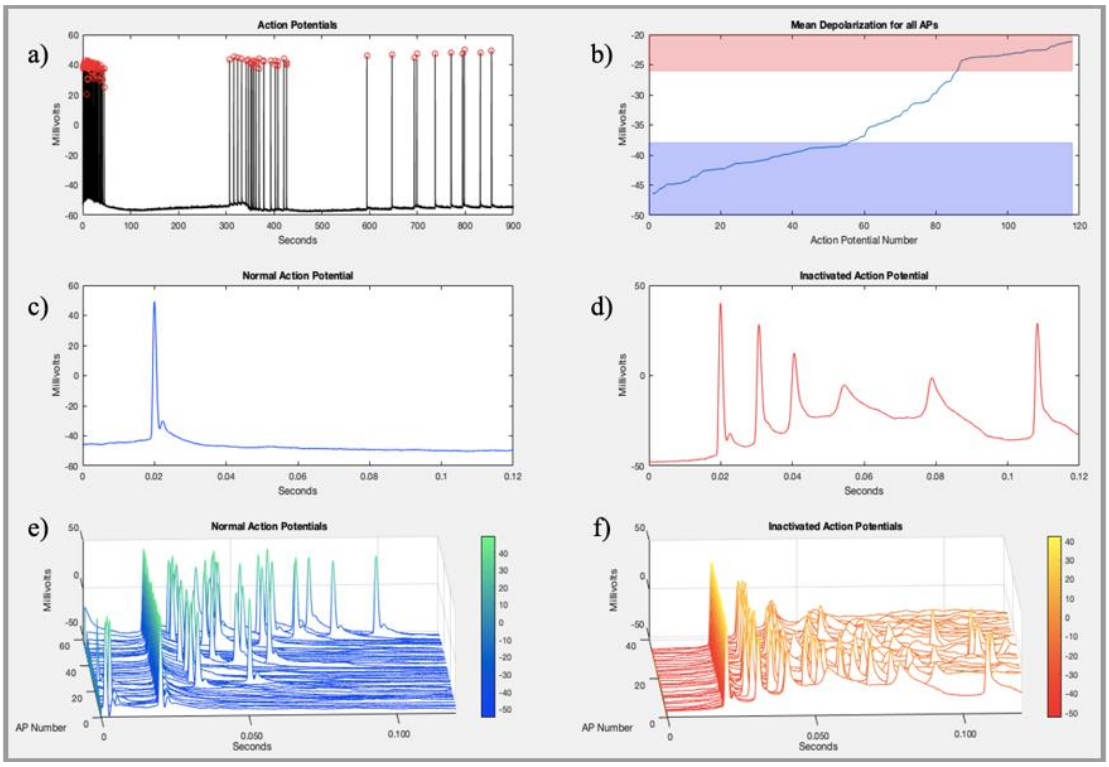

Figure 9. Action potential inactivation.

a) One hundred and eighteen action potential peaks were found in the first neuron in the intracellular recordings. b) The blue portion in this plot shows normal action potentials (elicited by lower levels of depolarization). The red portion shows action potentials that were inactivated due to a higher depolarization. c) Magnified view of a sample normal action potential. d) Magnified view of a sample inactivated action potential. Both waveforms shown in c) and d) lasted 0.12s. e) Depolarization levels did not affect action potential waveforms; thus, normal action potentials were recorded. f) Increased levels of depolarization affected action potential kinetics, resulting in inactivated action potentials.

One hundred and eighteen action potential peaks were found in the first neuron as indicated by the red dots. The mean depolarization for all action potentials from the first neuron can be seen in figure 7b. The blue portion of the figure demonstrates the number of action potentials that are normal due to low depolarization. There are fifty-five action potentials that were unaffected due to low depolarization in the blue portion. The red portion of the figure demonstrates the number of action potentials that are inactivated due to a higher depolarization. Thirty-two action potentials were affected by the high depolarization in the red portion. Since there is higher depolarization, the action potentials became more inactivated and distorted.

Magnified views of two different action potential firings due to depolarization can be seen in figure 7 c and d. Each action potential firing lasts 0.12 seconds. The action potential firing in 7c is considered normal, solitary firing where the pattern consists of a single spike, occasionally interspersed with periods of silence due to low depolarization. The action potential firing in ‘d’ is considered moderate duration a burst, where the pattern consists of a train of five to eight spikes, usually caused by higher depolarization. In this case, there are six action potential bursts in the same amount of time. The two magnified views of action potentials in two different moments in time showed the effect of depolarization on action potential inactivation. When there is low stimulation and depolarization as shown in 7c, the action potential firing was normal. When there is high stimulation and an increase in depolarization amplitude as shown in ‘d’, the action potential firing becomes more inactivated.

Each of the fifty-five normal-firing action potentials from the low depolarization blue portion of figure 7b can be seen in figure 7e. When a maximum threshold was set at -38 mV for the voltage of the depolarization, spontaneous depolarizations could not provide enough stimulation to affect action potential firing. Therefore, action potential firing was normal as seen in 7e.

Each of the thirty-two inactivated action potentials from the high depolarization red portion of figure 7b can be seen in figure 7f. When a minimum threshold was set at -26 mV for the voltage of the depolarization, spontaneous depolarizations could provide enough stimulation to affect action potential firing. Therefore, action potential firing became more inactivated as seen in 7f.

Similar figures for the second, third, and fourth neurons can be seen in the appendix figures. In each of the four neurons in the patient with idiopathic seizure disorder, a change in action potential activation can be seen depending on depolarization amplitude. Action potential inactivation can be seen in patients with idiopathic seizure disorder when the amplitude of depolarization was increased.

Figures for the other neurons that were not analyzed in this study can also be seen in the appendix figures.

DISCUSSION

Only a few studies have used intracortical fixed-geometry microelectrode arrays to analyze pathophysiological mechanisms in patients with intractable temporal lobe epilepsy [17], [32], [52]–[55], but these studies have provided unique and important insights. Here, *in vivo* extracellular microelectrode array recordings in epileptic patients have been combined with *in vitro* extracellular and intracellular recordings from resected tissue to study the spatiotemporal dynamics of interictal spikes as well as the mechanistic linkage between the profound paroxysmal depolarizations and the biophysical alterations in action potential generation. Using this approach, sequences of interictal spikes were found to consistently propagate across the epileptic cortex. It was also found that profound depolarizations similar to interictal spikes generated bursts of inactivated action potentials *in vitro*. Given that interictal spikes were shown to propagate consistently, it is proposed that the associated depolarization-induced action potential inactivation, also propagated consistently through the neocortex.

Depolarization-induced action potential inactivation

In vitro whole-cell recordings in a neocortical slice preparation of resected tissue were done to study action potential firing due to profound depolarizations. Action potentials (APs) recorded intracellularly from human neocortical tissue fired in bursts during depolarizations similar to interictal spikes. The APs at the start of a burst had typical AP

waveforms; however, as expected from previous *in vitro* brain slice studies, the AP waveforms displayed increased duration and decreased amplitude as the bursts progressed and the neurons underwent progressive depolarization, consistent with the definition of inactivated APs [29], [50], [51]. The extracellular microelectrode array recordings integrate signals from many neurons; therefore, the summation of inactivated AP firing from many nearby neurons contributes to the complex extracellularly recorded signals.

Propagation of interictal spikes and action potentials contributing to epileptogenesis.

Interictal spikes have been hypothesized to contribute to epileptogenesis by a mechanism that involves the formation of new synapses based on neuronal activity [56], [57]. . Interictal spikes have been observed to propagate through neocortical tissue during electrographic recordings [1], [53], [58]–[62]. Consistent with these studies, this data in the human epileptic cortex demonstrates the spatiotemporal propagation of interictal spikes, as well as the possible inactivation of action potentials by interictal spikes, as seen in the in vitro analysis. This supports a key element in the hypothesis that interictal spiks, and the associated action potential firing, may lead to the modification of synaptic circuits and contribute to the progression of epilepsy. Interictal spike depolarization provides a mechanism by which temporally and spatially correlated AP bursting can be triggered in a small area of the cortex. It is plausible that neurons in a cortical area with

large interictal spikes would develop aberrantly strong synaptic connections through Hebbian plasticity, and that this region of hyper-connectivity could be expanded through interictal spike propagation.

Laminar distribution of interictal spike depolarization levels.

Given the planarity of the microelectrode array and the curviform geometry of the implanted gyrus, it is plausible that electrodes around the middle of the array reached slightly deeper cortical layers. It was found that these electrodes recorded higher amplitude interictal spikes than outer electrodes. This distribution was observed in all interictal spikes over time and suggests that in addition to topographical propagation of interictal spikes across the cortex, there possibly exist highly coherent laminar dynamics in the spatial distribution patterns of interictal spikes. Given that action potential inactivation has been shown to correlate with paroxysmal depolarization levels, as found in the *in vitro* studies shown here, deeper cortical layers possibly have a more profound contribution to action potential inactivation. This could have implications for the recruitment patterns of neurons at different cortical depths into the epileptic network through synaptic strengthening, as interictal spikes propagate across the cortex.

CONCLUSION

In summary, the results here show that large interictal spike depolarizations *in vivo* could account for the bursts of action potential and action potential inactivation seen *in vitro*.

Large interictal spikes and their concomitant inactivated APs consistently propagated across the cortex on a submillimeter scale. Propagating interictal spikes with inactivated APs may contribute to the progression of epilepsy by generating and expanding regions of synaptic hyper-connectivity in the neocortex via Hebbian mechanisms [16], [53]–[56]. If the consistent propagation of inactivated action potentials recruits neocortical neurons into the aberrant epileptogenic networks through Hebbian plasticity, then propagating interictal spikes may be a clinically useful electrophysiological signature of epilepsy and its progression.

REFERENCES

[1] E. C. Conrad *et al.*, “Spatial distribution of interictal spikes fluctuates over time and localizes seizure onset,” *Brain*, vol. 143, no. 2, pp. 554–569, Feb. 2020, doi: 10.1093/brain/awz386.

[2] A. Katz, D. A. Marks, G. McCarthy, and S. S. Spencer, “Does interictal spiking change prior to seizures?,” *Electroencephalography and Clinical Neurophysiology*, vol. 79, no. 2, pp. 153–156, Aug. 1991, doi: 10.1016/0013-4694(91)90054-8.

[3] R. Efron, “THE EFFECT OF OLFACTORY STIMULI IN ARRESTING UNCINATE FITS,” *Brain*, vol. 79, no. 2, pp. 267–281, 1956, doi: 10.1093/brain/79.2.267.

[4] G. Alarcon, “Origin and propagation of interictal discharges in the acute electrocorticogram. Implications for pathophysiology and surgical treatment of temporal lobe epilepsy,” *Brain*, vol. 120, no. 12, pp. 2259–2282, Dec. 1997, doi: 10.1093/brain/120.12.2259.

[5] R. E. D. Bautista, M. A. Cobbs, D. D. Spencer, and S. S. Spencer, “Prediction of Surgical Outcome by Interictal Epileptiform Abnormalities During Intracranial EEG Monitoring in Patients with Extrahippocampal Seizures,” *Epilepsia*, vol. 40, no. 7, pp. 880–890, Jul. 1999, doi: 10.1111/j.1528-1157.1999.tb00794.x.

[6] A. Bragin, C. L. Wilson, R. J. Staba, M. Reddick, I. Fried, and J. Engel, “Interictal high-frequency oscillations (80-500Hz) in the human epileptic brain: Entorhinal cortex,” *Ann Neurol.*, vol. 52, no. 4, pp. 407–415, Oct. 2002, doi: 10.1002/ana.10291.

[7] W. T. Blume, “Current trends in electroencephalography:,” *Current Opinion in Neurology*, vol. 14, no. 2, pp. 193–197, Apr. 2001, doi: 10.1097/00019052-200104000-00010.

[8] K. J. Staley and F. E. Dudek, “Interictal Spikes and Epileptogenesis,” *Epilepsy Currents*, vol. 6, no. 6, pp. 199–202, Nov. 2006, doi: 10.1111/j.1535-7511.2006.00145.x.

[9] R. S. Fisher, H. E. Scharfman, and M. deCurtis, “How Can We Identify Ictal and Interictal Abnormal Activity?,” *Adv Exp Med Biol*, vol. 813, pp. 3–23, 2014, doi: 10.1007/978-94-017-8914-1_1.

[10] A. Hufnagel, M. Dümpelmann, J. Zentner, O. Schijns, and C. E. Elger, “Clinical relevance of quantified intracranial interictal spike activity in presurgical evaluation of epilepsy,” *Epilepsia*, vol. 41, no. 4, pp. 467–478, Apr. 2000, doi: 10.1111/j.1528-1157.2000.tb00191.x.

[11] E. D. Marsh *et al.*, “Interictal EEG spikes identify the region of electrographic seizure onset in some, but not all, pediatric epilepsy patients,” *Epilepsia*, vol. 51, no. 4, pp. 592–601, Apr. 2010, doi: 10.1111/j.1528-1167.2009.02306.x.

[12] E. Asano *et al.*, “Is intraoperative electrocorticography reliable in children with intractable neocortical epilepsy?,” *Epilepsia*, vol. 45, no. 9, pp. 1091–1099, Sep. 2004, doi: 10.1111/j.0013-9580.2004.65803.x.

[13] “Epileptiform-abnormalities.pdf.” .

[14] K. J. Staley, A. White, and F. E. Dudek, “Interictal spikes: Harbingers or causes of epilepsy?,” *Neuroscience Letters*, vol. 497, no. 3, pp. 247–250, Jun. 2011, doi: 10.1016/j.neulet.2011.03.070.

[15] P. J. Karoly *et al.*, “Interictal spikes and epileptic seizures: their relationship and underlying rhythmicity,” *Brain*, vol. 139, no. 4, pp. 1066–1078, Apr. 2016, doi: 10.1093/brain/aww019.

[16] K. J. Staley and F. E. Dudek, “Interictal Spikes and Epileptogenesis,” *Epilepsy Currents*, vol. 6, no. 6, pp. 199–202, Nov. 2006, doi: 10.1111/j.1535-7511.2006.00145.x.

[17] C. J. Keller *et al.*, “Heterogeneous neuronal firing patterns during interictal epileptiform discharges in the human cortex,” *Brain*, vol. 133, no. 6, pp. 1668–1681, Jun. 2010, doi: 10.1093/brain/awq112.

[18] C. J. Keller *et al.*, “Heterogeneous neuronal firing patterns during interictal epileptiform discharges in the human cortex,” *Brain*, vol. 133, no. 6, pp. 1668–1681, Jun. 2010, doi: 10.1093/brain/awq112.

[19] E. D. Marsh *et al.*, “Interictal EEG spikes identify the region of electrographic seizure onset in some, but not all, pediatric epilepsy patients,” *Epilepsia*, vol. 51, no. 4, pp. 592–601, Apr. 2010, doi: 10.1111/j.1528-1167.2009.02306.x.

[20] B. Maharathi *et al.*, “Interictal spike connectivity in human epileptic neocortex,” *Clinical Neurophysiology*, vol. 130, no. 2, pp. 270–279, Feb. 2019, doi: 10.1016/j.clinph.2018.11.025.

[21] G. Alarcon, “Electrophysiological aspects of interictal and ictal activity in human partial epilepsy,” *Seizure*, vol. 5, no. 1, pp. 7–33, Mar. 1996, doi: 10.1016/S1059-1311(96)80014-8.

[22] A. Korzeniewska *et al.*, “Ictal propagation of high frequency activity is recapitulated in interictal recordings: Effective connectivity of epileptogenic networks recorded with intracranial EEG,” *NeuroImage*, vol. 101, pp. 96–113, Nov. 2014, doi: 10.1016/j.neuroimage.2014.06.078.

[23] R. Krendl, S. Lurger, and C. Baumgartner, “Absolute spike frequency predicts surgical outcome in TLE with unilateral hippocampal atrophy,” *Neurology*, vol. 71, no. 6, pp. 413–418, Aug. 2008, doi: 10.1212/01.wnl.0000310775.87331.90.

[24] J. W. Miller and J. Gotman, “The meaning of interictal spikes in temporal lobe epilepsy: Should we count them?,” *Neurology*, vol. 71, no. 6, pp. 392–393, Aug. 2008, doi: 10.1212/01.wnl.0000324256.00488.69.

[25] G. Alarcon, “Electrophysiological aspects of interictal and ictal activity in human partial epilepsy,” *Seizure*, vol. 5, no. 1, pp. 7–33, Mar. 1996, doi: 10.1016/S1059-1311(96)80014-8.

[26] A. Hufnagel, M. Dumpelmann, J. Zentner, O. Schijns, and C. E. Elger, “Clinical Relevance of Quantified Intracranial Interictal Spike Activity in Presurgical Evaluation of Epilepsy,” *Epilepsia*, vol. 41, no. 4, pp. 467–478, Apr. 2000, doi: 10.1111/j.1528-1157.2000.tb00191.x.

[27] F. Rosenow and H. Luders, “Presurgical evaluation of epilepsy,” p. 18.

[28] P. A. Schwartzkroin and D. A. Prince, “Effects of TEA on hippocampal neurons,” *Brain Res*, vol. 185, no. 1, pp. 169–181, Mar. 1980, doi: 10.1016/0006-8993(80)90680-0.

[29] E. R. Kandel and W. A. Spencer, “Electrophysiology of hippocampal neurons. II. After-potentials and repetitive firing,” *J Neurophysiol*, vol. 24, pp. 243–259, May 1961, doi: 10.1152/jn.1961.24.3.243.

[30] P. A. House, J. D. MacDonald, P. A. Tresco, and R. A. Normann, “Acute microelectrode array implantation into human neocortex: preliminary technique and histological considerations,” *Neurosurg Focus*, vol. 20, no. 5, p. E4, May 2006, doi: 10.3171/foc.2006.20.5.5.

[31] L. R. Hochberg *et al.*, "Neuronal ensemble control of prosthetic devices by a human with tetraplegia," *Nature*, vol. 442, no. 7099, Art. no. 7099, Jul. 2006, doi: 10.1038/nature04970.

[32] A. Waziri, C. A. Schevon, J. Cappell, R. G. Emerson, G. M. McKhann, and R. R. Goodman, "Initial surgical experience with a dense cortical microarray in epileptic patients undergoing craniotomy for subdural electrode implantation," *Neurosurgery*, vol. 64, no. 3, pp. 540–545, Mar. 2009, doi: 10.1227/01.NEU.0000337575.63861.10.

[33] J. D. Simeral, S.-P. Kim, M. J. Black, J. P. Donoghue, and L. R. Hochberg, "Neural control of cursor trajectory and click by a human with tetraplegia 1000 days after implant of an intracortical microelectrode array," *J Neural Eng*, vol. 8, no. 2, p. 025027, Apr. 2011, doi: 10.1088/1741-2560/8/2/025027.

[34] S. Suner, M. R. Fellows, C. Vargas-Irwin, G. K. Nakata, and J. P. Donoghue, "Reliability of signals from a chronically implanted, silicon-based electrode array in non-human primate primary motor cortex," *IEEE Trans Neural Syst Rehabil Eng*, vol. 13, no. 4, pp. 524–541, Dec. 2005, doi: 10.1109/TNSRE.2005.857687.

[35] D. Hermes, K. J. Miller, H. J. Noordmans, M. J. Vansteensel, and N. F. Ramsey, "Automated electrocorticographic electrode localization on individually rendered brain surfaces," *J Neurosci Methods*, vol. 185, no. 2, pp. 293–298, Jan. 2010, doi: 10.1016/j.jneumeth.2009.10.005.

[36] M. de Curtis and G. Avanzini, "Interictal spikes in focal epileptogenesis," *Progress in Neurobiology*, vol. 63, no. 5, pp. 541–567, Apr. 2001, doi: 10.1016/S0301-0082(00)00026-5.

[37] G. E. Chatrian, C.-M. Shaw, and H. Leffman, "The significance of periodic lateralized epileptiform discharges in EEG: An electrographic, clinical and pathological study," *Electroencephalography and Clinical Neurophysiology*, vol. 17, no. 2, pp. 177–193, Aug. 1964, doi: 10.1016/0013-4694(64)90149-X.

[38] J. Gotman, "Quantitative measurements of epileptic spike morphology in the human EEG," *Electroencephalography and Clinical Neurophysiology*, vol. 48, no. 5, pp. 551–557, May 1980, doi: 10.1016/0013-4694(80)90290-4.

[39] K. A. Kooi, "Voltage-time characteristics of spikes and other rapid electroencephalographic transients: semantic and morphological considerations," *Neurology*, vol. 16, no. 1, pp. 59–66, Jan. 1966, doi: 10.1212/wnl.16.1.59.

[40] S. F. Traynelis and R. Dingledine, “Potassium-induced spontaneous electrographic seizures in the rat hippocampal slice,” *J Neurophysiol*, vol. 59, no. 1, pp. 259–276, Jan. 1988, doi: 10.1152/jn.1988.59.1.259.

[41] R. J. Gumnit, H. Matsumoto, and C. Vasconetto, “DC activity in the depth of an experimental epiletic focus,” *Electroencephalography and Clinical Neurophysiology*, vol. 28, no. 4, pp. 333–339, Apr. 1970, doi: 10.1016/0013-4694(70)90225-7.

[42] B. Albowitz and U. Kuhnt, “Epileptiform activity in the guinea-pig neocortical slice spreads preferentially along supragranular layers--recordings with voltage-sensitive dyes,” *Eur J Neurosci*, vol. 7, no. 6, pp. 1273–1284, Jun. 1995, doi: 10.1111/j.1460-9568.1995.tb01117.x.

[43] H. Pockberger, P. Rappelsberger, and H. Petsche, “Penicillin-induced epileptic phenomena in the rabbit’s neocortex I. The development of interictal spikes after epicortical application of penicillin,” *Brain Res*, vol. 309, no. 2, pp. 247–260, Sep. 1984, doi: 10.1016/0006-8993(84)90591-2.

[44] C. E. Elger, E. J. Speckmann, O. Prohaska, and H. Caspers, “Pattern of intracortical potential distribution during focal interictal epileptiform discharges (FIED) and its relation to spinal field potentials in the rat,” *Electroencephalogr Clin Neurophysiol*, vol. 51, no. 4, pp. 393–402, Apr. 1981, doi: 10.1016/0013-4694(81)90103-6.

[45] J. S. Ebersole and A. B. Chatt, “Laminar interactions during neocortical epileptogenesis,” *Brain Res*, vol. 298, no. 2, pp. 253–271, Apr. 1984, doi: 10.1016/0006-8993(84)91425-2.

[46] J. S. Ebersole and R. A. Levine, “Abnormal neuronal responses during evolution of a penicillin epileptic focus in cat visual cortex,” *J Neurophysiol*, vol. 38, no. 2, pp. 250–256, Mar. 1975, doi: 10.1152/jn.1975.38.2.250.

[47] E. S. Goldensohn and D. P. Purpura, “Intracellular potentials of cortical neurons during focal epileptogenic discharges,” *Science*, vol. 139, no. 3557, pp. 840–842, Mar. 1963, doi: 10.1126/science.139.3557.840.

[48] M. J. Gutnick, B. W. Connors, and D. A. Prince, “Mechanisms of neocortical epileptogenesis in vitro,” *J Neurophysiol*, vol. 48, no. 6, pp. 1321–1335, Dec. 1982, doi: 10.1152/jn.1982.48.6.1321.

[49] D. Johnston and T. H. Brown, “The synaptic nature of the paroxysmal depolarizing shift in hippocampal neurons,” *Ann Neurol*, vol. 16 Suppl, pp. S65-71, 1984, doi: 10.1002/ana.410160711.

[50] D. Paré, M. deCurtis, and R. Llinás, “Role of the hippocampal-entorhinal loop in temporal lobe epilepsy: extra- and intracellular study in the isolated guinea pig brain in vitro,” *J Neurosci*, vol. 12, no. 5, pp. 1867–1881, May 1992.

[51] A. L. Hodgkin and A. F. Huxley, “The dual effect of membrane potential on sodium conductance in the giant axon of Loligo,” *J Physiol*, vol. 116, no. 4, pp. 497–506, Apr. 1952.

[52] W. Truccolo *et al.*, “Single-neuron dynamics in human focal epilepsy,” *Nature Neuroscience*, vol. 14, no. 5, Art. no. 5, May 2011, doi: 10.1038/nn.2782.

[53] C. A. Schevon, R. R. Goodman, G. McKhann, and R. G. Emerson, “Propagation of epileptiform activity on a submillimeter scale,” *J Clin Neurophysiol*, vol. 27, no. 6, pp. 406–411, Dec. 2010, doi: 10.1097/WNP.0b013e3181fdf8a1.

[54] C. A. Schevon, A. J. Trevelyan, C. E. Schroeder, R. R. Goodman, G. McKhann, and R. G. Emerson, “Spatial characterization of interictal high frequency oscillations in epileptic neocortex,” *Brain*, vol. 132, no. Pt 11, pp. 3047–3059, Nov. 2009, doi: 10.1093/brain/awp222.

[55] C. A. Schevon *et al.*, “Microphysiology of epileptiform activity in human neocortex,” *J Clin Neurophysiol*, vol. 25, no. 6, pp. 321–330, Dec. 2008, doi: 10.1097/WNP.0b013e31818e8010.

[56] K. Staley, J. L. Hellier, and F. E. Dudek, “Do Interictal Spikes Drive Epileptogenesis?,” *Neuroscientist*, vol. 11, no. 4, pp. 272–276, Aug. 2005, doi: 10.1177/1073858405278239.

[57] K. J. Staley and F. E. Dudek, “Interictal Spikes and Epileptogenesis,” *Epilepsy Currents*, vol. 6, no. 6, pp. 199–202, Nov. 2006, doi: 10.1111/j.1535-7511.2006.00145.x.

[58] R. G. Emerson, C. A. Turner, T. A. Pedley, T. S. Walczak, and M. Forgione, “Propagation patterns of temporal spikes,” *Electroencephalogr Clin Neurophysiol*, vol. 94, no. 5, pp. 338–348, May 1995, doi: 10.1016/0013-4694(94)00316-d.

[59] I. Merlet, L. Garcia–Larrea, M. C. Grégoire, F. Lavenne, and F. Mauguière, “Source propagation of interictal spikes in temporal lobe epilepsy: Correlations between

spike dipole modelling and [^{18} F]fluorodeoxyglucose PET data," *Brain*, vol. 119, no. 2, pp. 377–392, 1996, doi: 10.1093/brain/119.2.377.

[60] S. B. Tomlinson, C. Bermudez, C. Conley, M. W. Brown, B. E. Porter, and E. D. Marsh, "Spatiotemporal Mapping of Interictal Spike Propagation: A Novel Methodology Applied to Pediatric Intracranial EEG Recordings," *Front. Neurol.*, vol. 7, Dec. 2016, doi: 10.3389/fneur.2016.00229.

[61] G. Alarcon, "Origin and propagation of interictal discharges in the acute electrocorticogram. Implications for pathophysiology and surgical treatment of temporal lobe epilepsy," *Brain*, vol. 120, no. 12, pp. 2259–2282, Dec. 1997, doi: 10.1093/brain/120.12.2259.

[62] I. Ulbert, G. Heit, J. Madsen, G. Karmos, and E. Halgren, "Laminar analysis of human neocortical interictal spike generation and propagation: current source density and multiunit analysis in vivo," *Epilepsia*, vol. 45 Suppl 4, pp. 48–56, 2004, doi: 10.1111/j.0013-9580.2004.04011.x.

APPENDIX A.

MISCELLANEOUS FIGURES

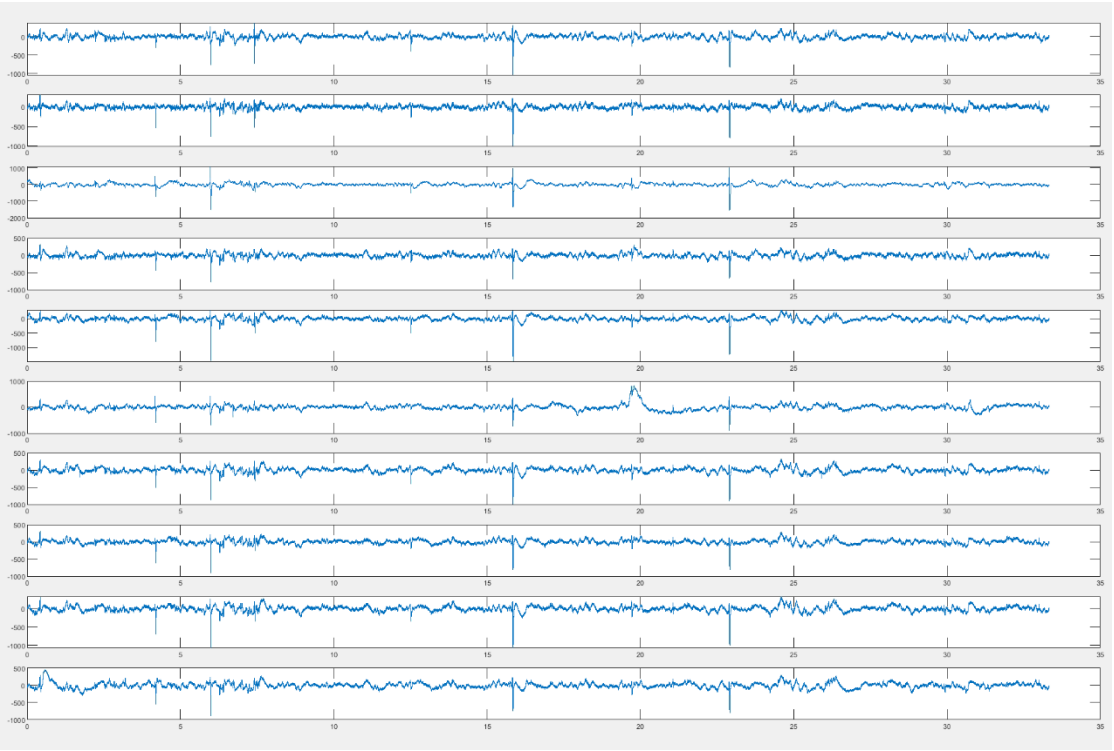

Recorded broadband data from 10 channels. As shown, sequences of interictal spikes (with profound negative deflection) can be seen across all electrodes within the same time segment. These were extracted using a windowing method for visual evaluation and subsequent analysis to map out propagation directions across the microelectrode array for different time segments.

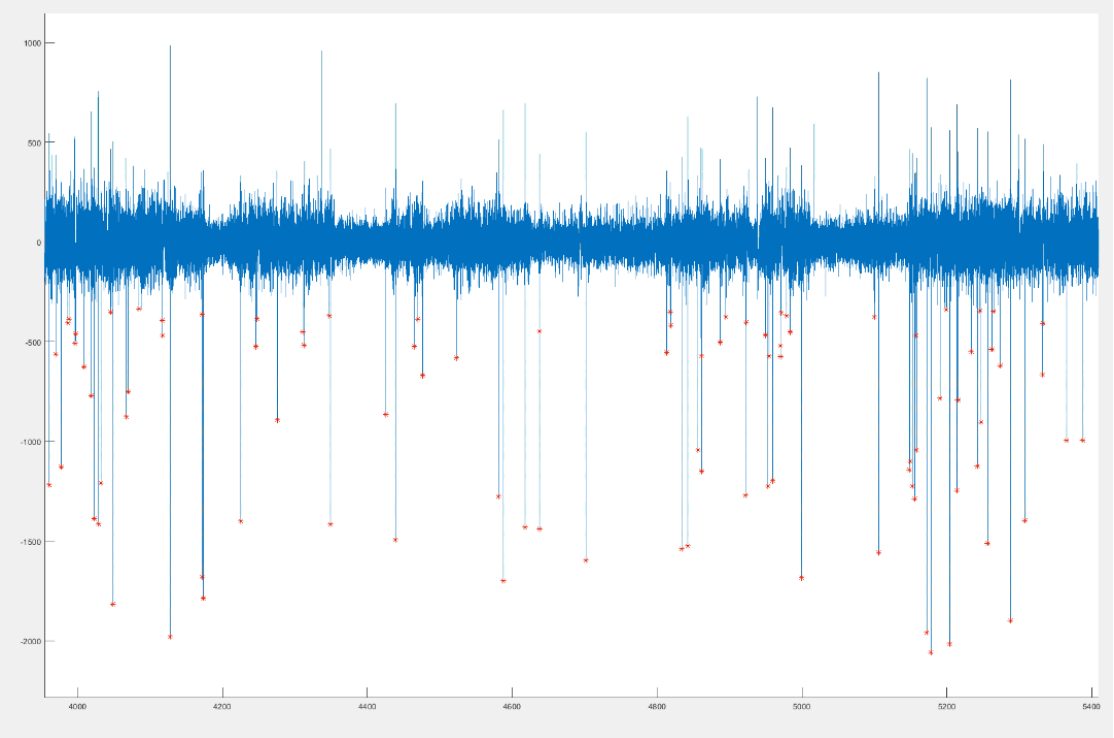

Data from a single recorded channel in the microelectrode array. Thresholding was used to identify candidate waveforms for visual evaluation. Waveforms which met the kinetic conditions discussed above were detected by the algorithm (red asterisks) for evaluation. The main features of interest were the negative going peak, and peak prominence.

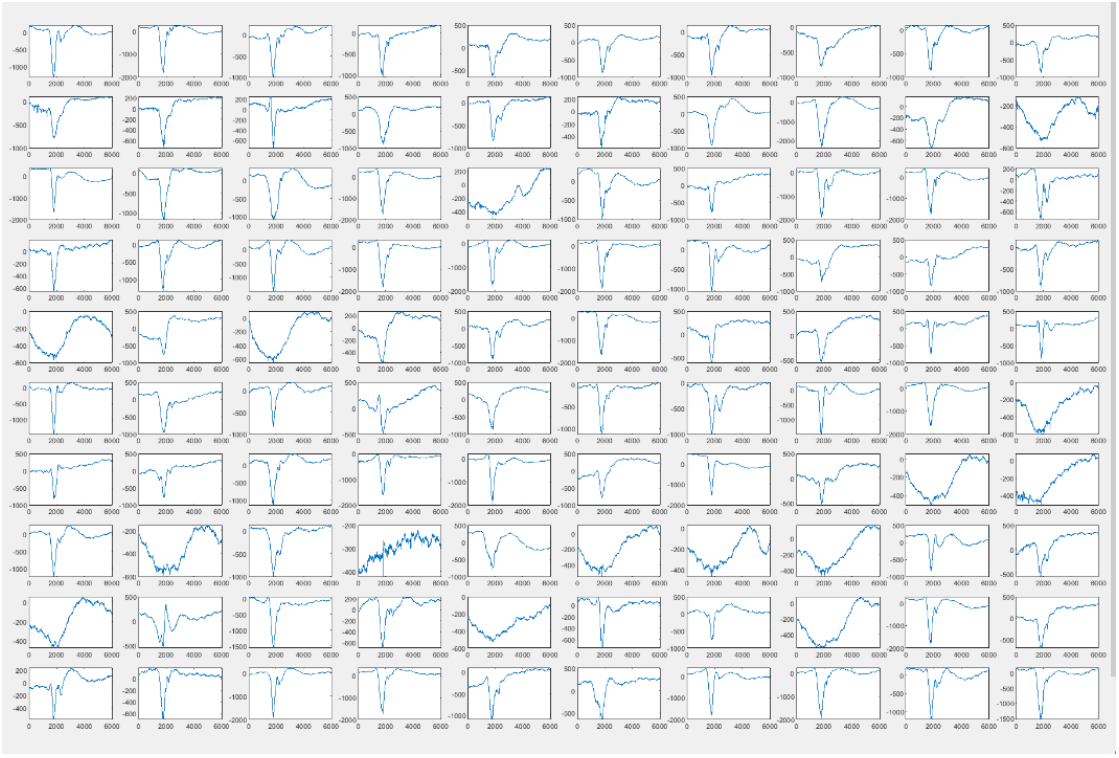

Sample waveforms from a single channel, after thresholding, prior to visual evaluation to remove artefactual waveforms. Waveforms which clearly do not fall into the interictal spike category based on kinetic features discussed can be seen. These were discarded.

Sample interictal spike with well-defined peak and morphology across the microelectrode array.

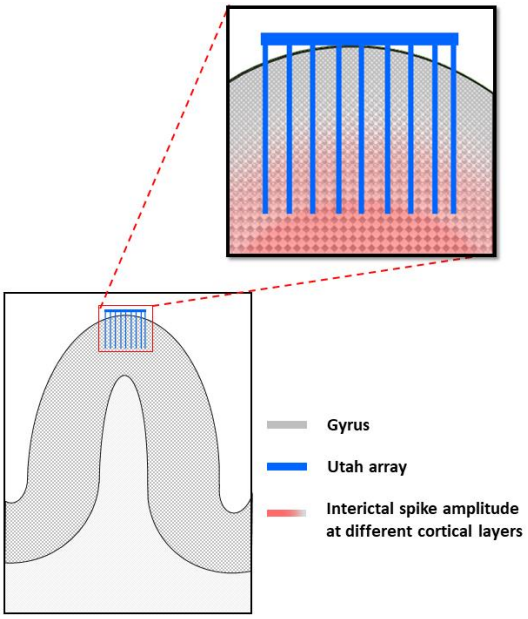

A graphical illustration of gyral anatomy, with implanted microelectrode array (not drawn to scale). Given the fixed geometry of the microelectrode array and the curviform morphology of the gyrus, it is plausible that electrodes in the middle of the array reached deeper cortical layers. These depths were found to have larger interictal spike depolarizations, possibly suggesting a more profound contribution of these layers to action potential inactivation and aberrant synaptic strengthening as interictal spikes propagate across the cortex.

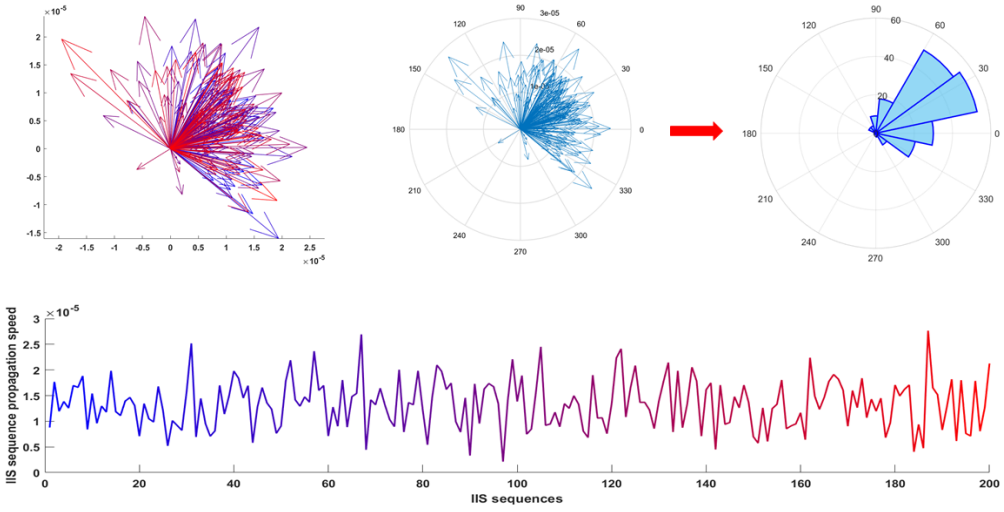

The top row depicts interictal spike propagation. The colored compass plot shows interictal spike propagation direction over time. The middle plot shows the original compass plot, while the far-right plot gives a circular histogram representation of interictal spike propagation directions (in degrees), where (0°=anterior, 90°=dorsal, 180°=posterior, 270°=ventral). The bottom graph shows a plot of propagation speed against time.

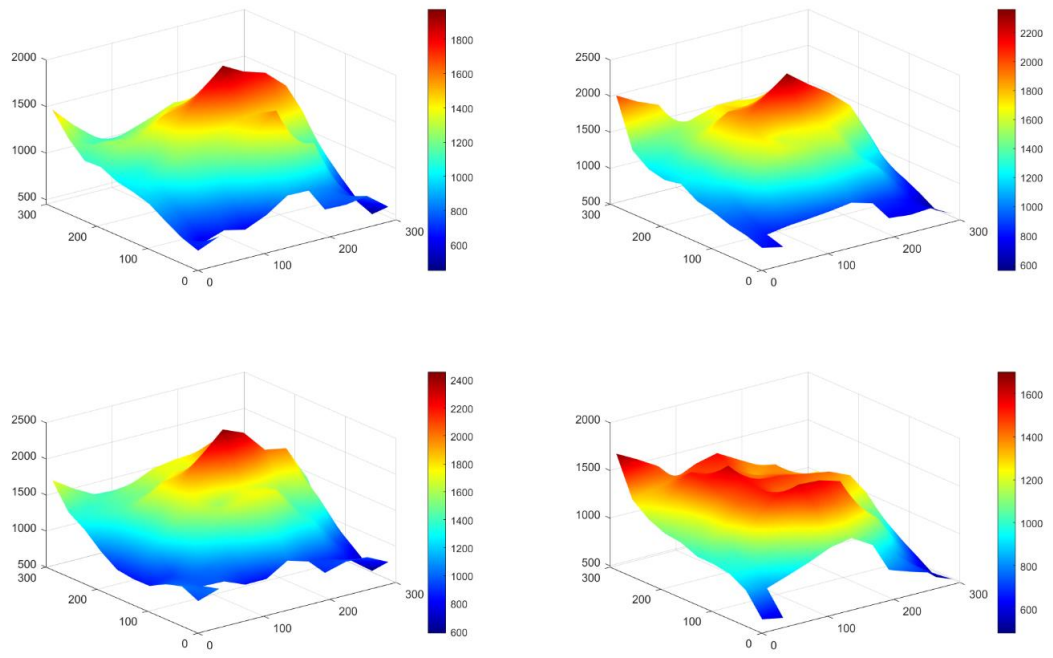

3D plot of four propagating interictal spikes across the microelectrode array

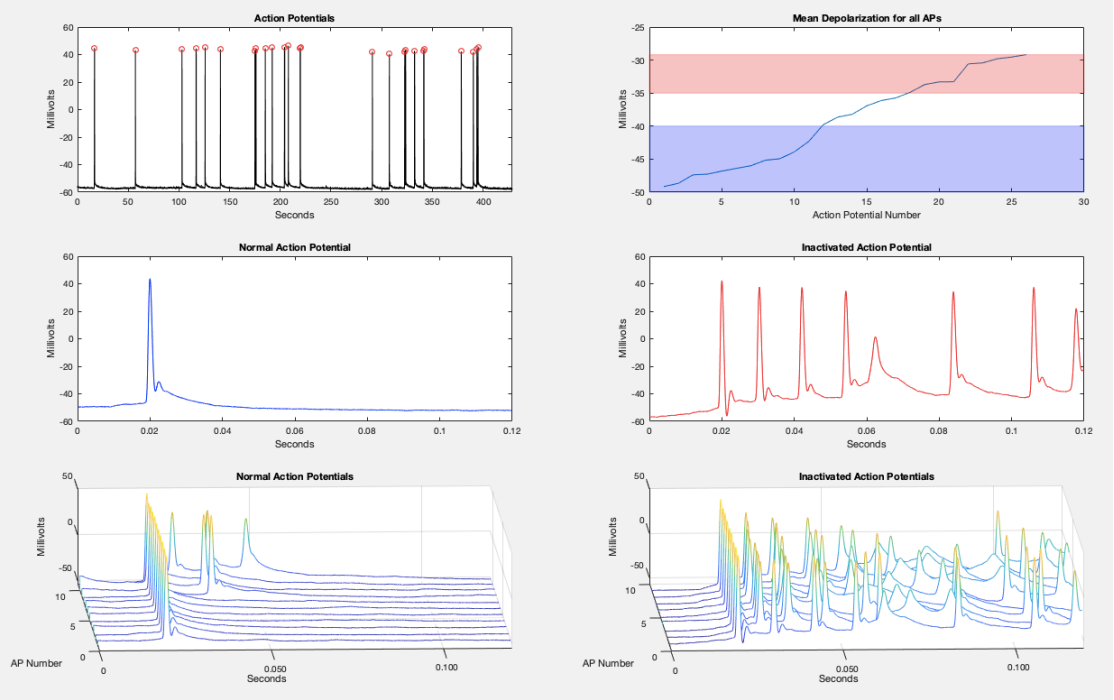

The figure shows each of the action potential peaks found in the second neuron as indicated by the red dots in the top left figure. The voltage of the interictal spikes slowly increases from zero to twenty-five milliseconds due to the fact that there is not a strong interictal spike depolarization. When a maximum threshold was set, spontaneous depolarizations could not provide enough stimulation to affect action potential firing. Therefore, action potential firing was normal and not inactivated. When a minimum threshold was set, spontaneous depolarizations could provide enough stimulation to affect action potential firing. Therefore, action potential firing became more inactivated.

45

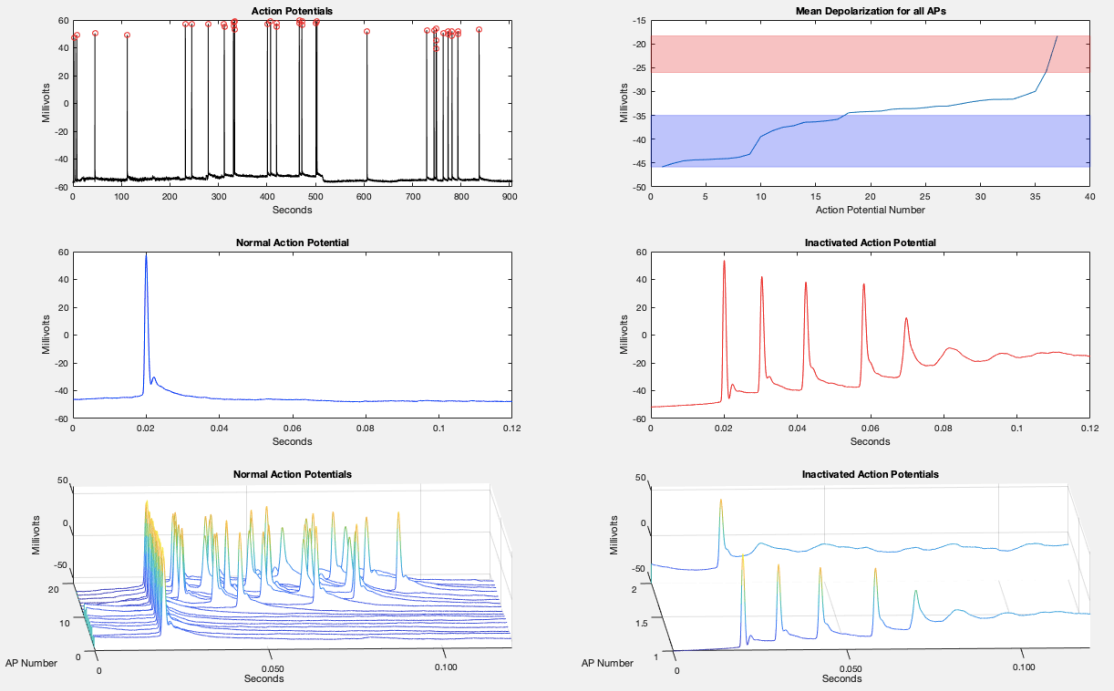

The figure shows each of the action potential peaks found in the third neuron as indicated by the red dots in the top left figure. The voltage of the interictal spikes slowly increases from zero to twenty-five milliseconds due to the fact that there is not a strong interictal spike depolarization. When a maximum threshold was set, spontaneous depolarizations could not provide enough stimulation to affect action potential firing. Therefore, action potential firing was normal and not inactivated. When a minimum threshold was set, spontaneous depolarizations could provide enough stimulation to affect action potential firing. Therefore, action potential firing became more inactivated.

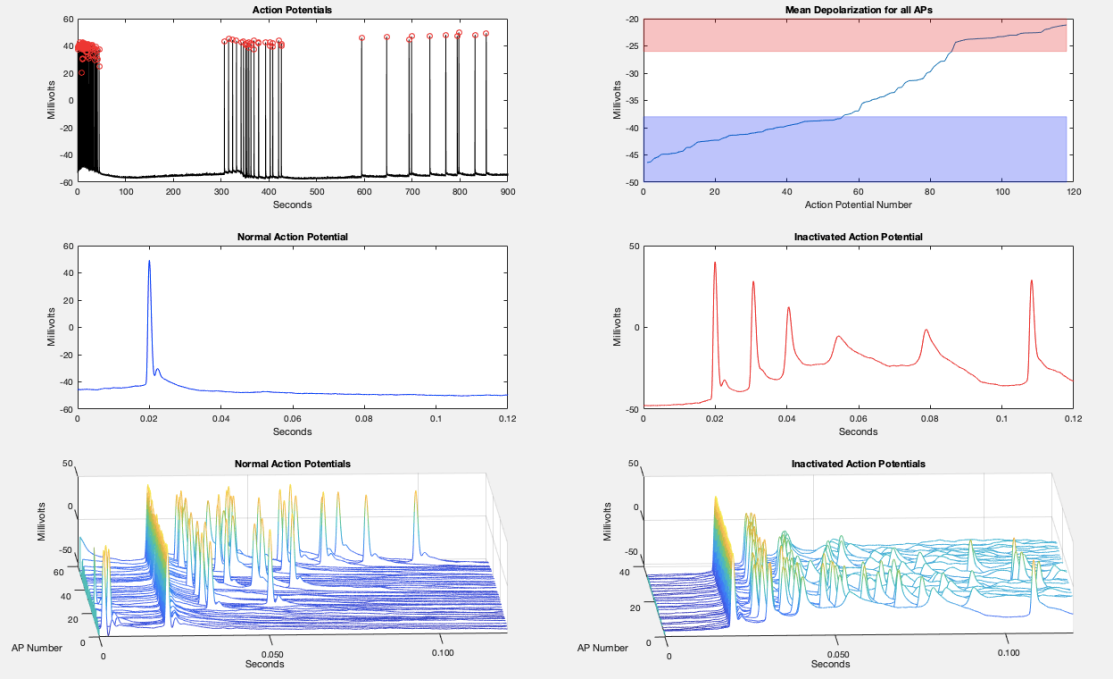

The figure shows each of the action potential peaks found in the fourth neuron as indicated by the red dots in the top left figure. The voltage of the interictal spikes slowly increases from zero to twenty-five milliseconds due to the fact that there is not a strong interictal spike depolarization. When a maximum threshold was set, spontaneous depolarizations could not provide enough stimulation to affect action potential firing. Therefore, action potential firing was normal and not inactivated. When a minimum threshold was set, spontaneous depolarizations could provide enough stimulation to affect action potential firing. Therefore, action potential firing became more inactivated.

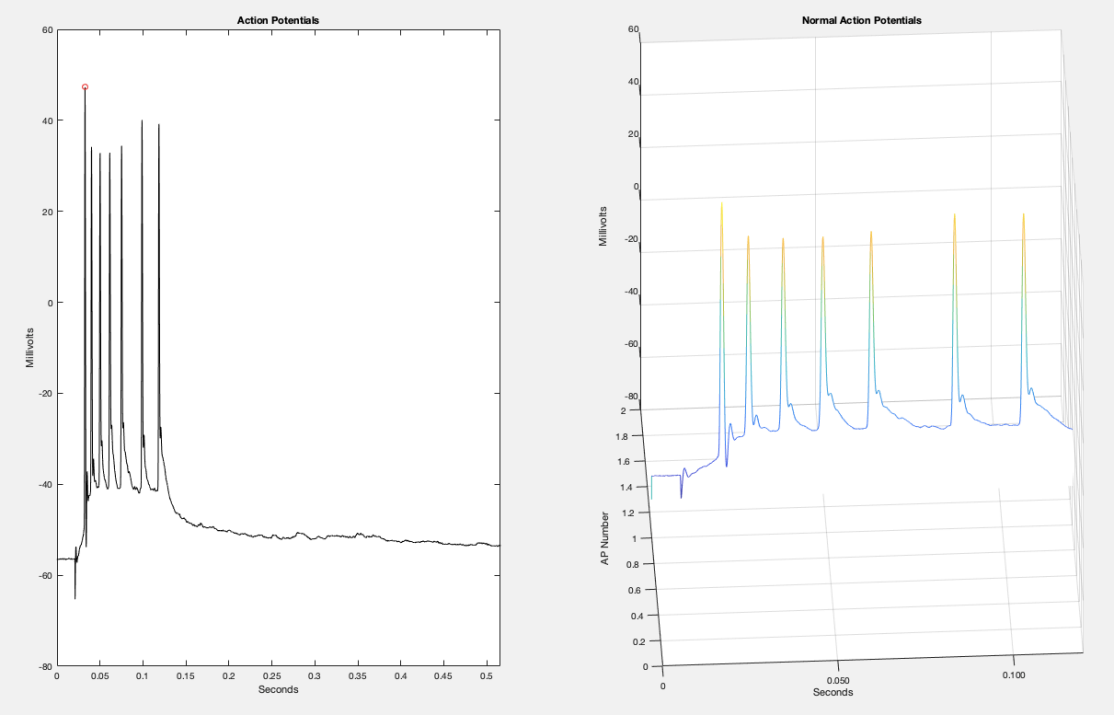

The figure shows each of the action potential peaks found in the sixth neuron as indicated by the red dots. When a maximum threshold was set, spontaneous depolarizations could not provide enough stimulation to affect action potential firing. Therefore, action potential firing was normal and not inactivated.

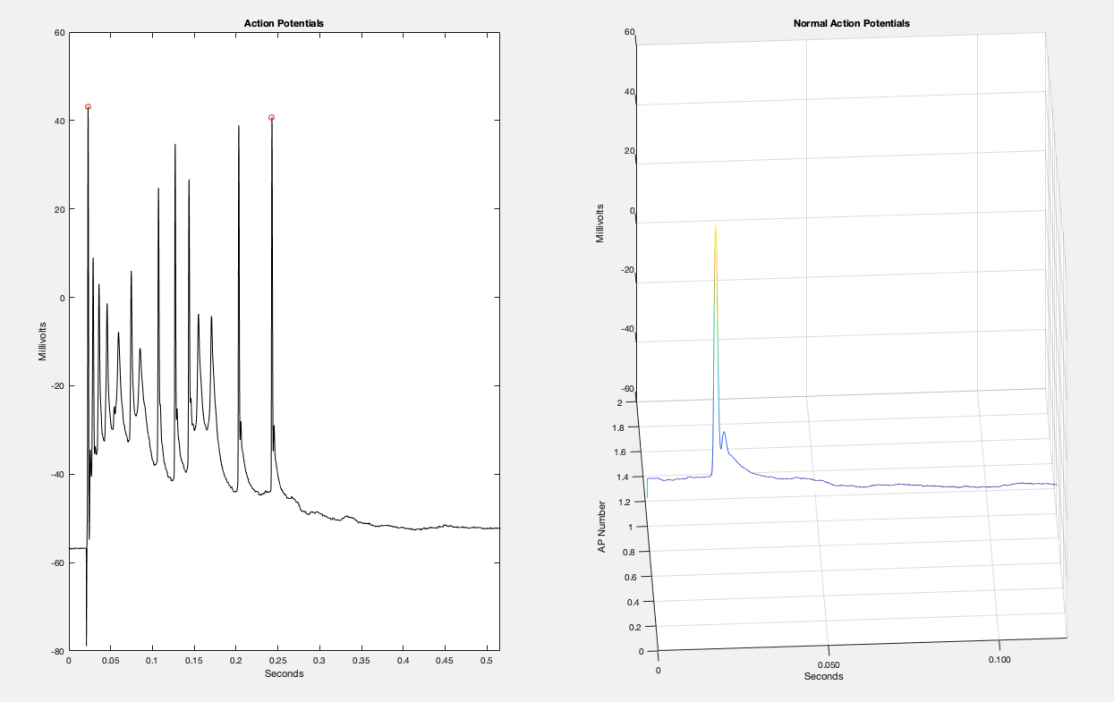

The figure shows each of the action potential peaks found in the seventh neuron as indicated by the red dots. When a maximum threshold was set, spontaneous depolarizations could not provide enough stimulation to affect action potential firing. Therefore, action potential firing was normal and not inactivated.

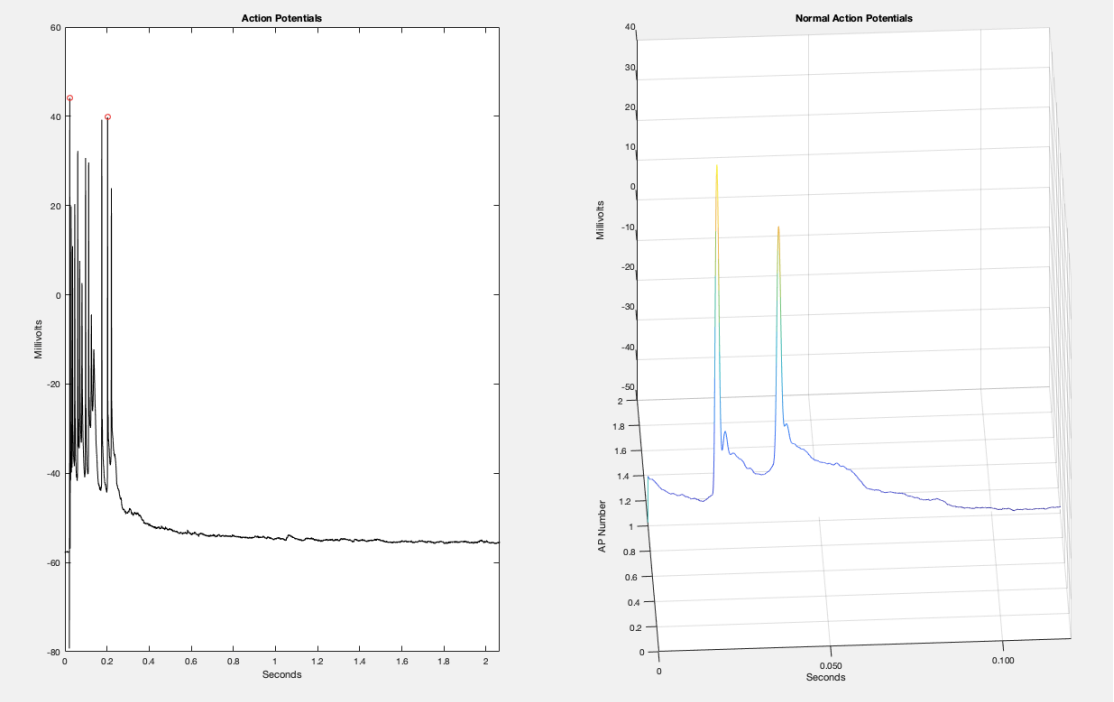

The figure shows each of the action potential peaks found in the eighth neuron as indicated by the red dots. When a maximum threshold was set, spontaneous depolarizations could not provide enough stimulation to affect action potential firing. Therefore, action potential firing was normal and not inactivated.

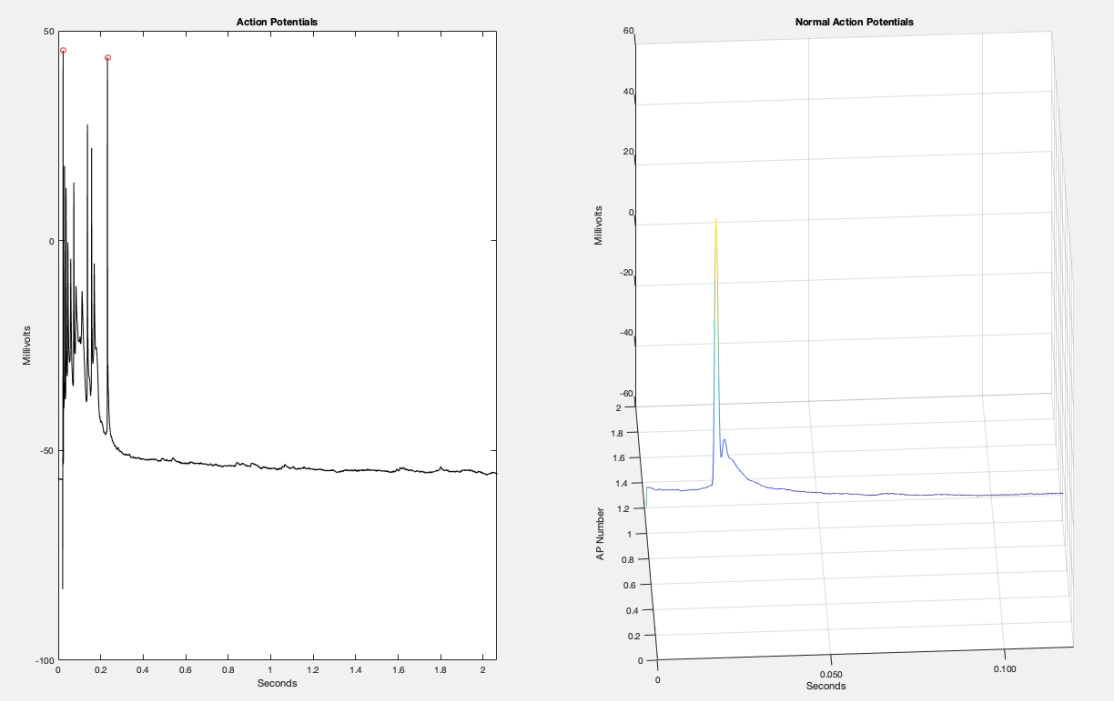

The figure shows each of the action potential peaks found in the ninth neuron as indicated by the red dots. When a maximum threshold was set, spontaneous depolarizations could not provide enough stimulation to affect action potential firing. Therefore, action potential firing was normal and not inactivated.

APPENDIX B.

MATLAB ANALYSIS CODE

```
%% load data
% addpath 'E:\human CNS\UU\gamma\20080623-203922';
% save('patient07_data','Chan_IIS_SnippetIdxs','times','Chan','NP_times'); %
after running script, save specific variables of interest
load('20080623-203922-006.mat');
%% bandpass filtering
d1 = designfilt('bandpassfir','FilterOrder',10, ...
         'CutoffFrequency1',1,'CutoffFrequency2',50, ...
         'SampleRate',30000);
filtered_sig=filtfilt(d1,sig_1ch);

chan2use=1; % channel from data
raw_sig_chanx = NS5.Data(chan2use,:); % extract from 11300000 to omit
preceeding artefactual samples

IIS_lfp_filter = designfilt('bandpassfir','FilterOrder',10, ... % design
bandpass filter (0.5-50Hz) to extract lfp from data
         'CutoffFrequency1',0.5,'CutoffFrequency2',50,'SampleRate',30000);
Filt_Chan_Sig=filtfilt(IIS_lfp_filter,raw_sig_chanx); % implement BP filter
figure;
plot(raw_sig_chanx); hold on;plot(Filt_Chan_Sig); % visualize filtered signal
(lfp)
legend('original','filtered')

%% detection of negative peaks
thresholdAmplitude = 4*std(Filt_Chan_Sig); % set threshold for peak detection
to -4 standard deviations
```

```
TF =
islocalmin(Filt_Chan_Sig,'MinProminence',round(thresholdAmplitude),'MinSeparati
on',6000,'MaxNumExtrema',300); % find treshold crossings of interest
NegPeak_indexes = find(TF); % find indexes of detected peaks
NegPeaks=Filt_Chan_Sig(NegPeak_indexes); % extract detected peaks (amplitudes)
from original signal

FsNew = 30000;snippetTimeLength = 0.2;  %snippet length=snippetTimeLength ms
(eg. 200ms)
Snippet_window = round((-0.3*FsNew*snippetTimeLength-
1):(0.7*FsNew*snippetTimeLength));  %array to store locations of samples around
each peak
Chan_IIS_SnippetIdxs = repmat
(Snippet_window,length(NegPeak_indexes),1)+NegPeak_indexes';  %uses locations
of peaks (actualNegPeakLocs) to find locations of samples around each peak
Chan_IIS_Snippets = Filt_Chan_Sig(Chan_IIS_SnippetIdxs);  %uses sample indexes
to find and extract sample amplitudes
figure;plot(Chan_IIS_Snippets');

candidate_IIS=Chan_IIS_Snippets;

% visualize detected waveforms for evaluation
rowNum=0;
for f=1:3
    figure
    for s=1:100
        subplot(10,10,s)
        plot(Chan_IIS_Snippets(rowNum+s,:)),title(string(rowNum+s));
```

```
    end
    rowNum=rowNum+100;
end

to_rm = [25,29,43:45,47,50,55,59,71,73:75,84,95,96,104,129,132,133,138,140:142
...

,152,157,161,177,200,220,225,238,241,243,248,260,269,270,272,274,276:278,281,28
2,285,288]; % artefactual waveforms to remove
% remove artefactual waveforms
candidate_IIS(to_rm,:)=[]; % waveforms of interest
NegPeak_indexes(to_rm)=[];Chan_IIS_SnippetIdxs(to_rm,:)=[];
Chan_IIS_Snippets(to_rm,:)=[];

% extract IIS info from all channels and store them in struct 'Chan'
for k=1:96
    raw_sig_chanx = NS5.Data(k,:);
    Filt_Chan_Sig=filtfilt(IIS_lfp_filter,raw_sig_chanx); % implement BP filter
    Chan(k).Snippets = Filt_Chan_Sig(Chan_IIS_SnippetIdxs);  %uses sample
indexes to find and extract sample amplitudes
    for j=1:size(Chan(k).Snippets,1)
        [NP_amplitudes(k,j),~]=findpeaks (-
Chan(k).Snippets(j,:),times(Chan_IIS_SnippetIdxs(j,:)),'NPeaks',1,'SortStr','de
scend'); % extract negative peak amplitudes and times
    end
end

%% visualize interictal spike sequences
```

```
arr_map=[1   2    nan nan nan nan 8    10   14   4;
         65  66   33  34  7    9    11   12   16   18;
         67  68   35  36  5    17   13   23   20   22;
         69  70   37  38  48   15   19   25   27   24;
         71  72   39  40  42   50   54   21   29   26;
         73  74   41  43  44   46   52   62   31   28;
         75  76   45  47  51   56   58   60   64   30;
         77  78   82  49  53   55   57   59   61   32;
         79  80   84  86  87   89   91   94   63   95;
         3   81   83  85  88   90   92   93   96   6]';
h=1:10;
for f=1:10
    figure,
    for k=1:100
        subplot(10,10,k),sequenceNum=h(f);
        if ~isnan(arr_map(k))
            % plot snippets against their original indexes in the raw signal

plot(Chan_IIS_SnippetIdxs(sequenceNum,:),Chan(arr_map(k)).Snippets(sequenceNum,
:)),hold on;
            % values in NP_times field are in sec; convert them to original
indexes by multiplying by sampling freq
            plot(FsNew*Chan(arr_map(k)).NP_times(sequenceNum),-
Chan(arr_map(k)).NP_amplitudes(sequenceNum),'*');
            if arr_map(k)==1 % use title of first subplot to display IIS
sequence no.
                title(['IIS sequence' num2str(sequenceNum)]); % insert IIS
sequence no. as title of first plot
```

```
            else
                title(['channel ' num2str(arr_map(k))]); %add channel number
            end
        end
    end
end

% arr_map_transp=arr_map'; % transpose arr_map
h=0;
for f=1:2
    figure
    for k=1:25
%         sequenceNum=k+h;
%         avgMiddleFour=(NP_times(42,sequenceNum)+NP_times(44,sequenceNum)...
%             +NP_times(46,sequenceNum)+NP_times(50,sequenceNum))./4;
%         negPeakTimes=(NP_times-avgMiddleFour);
        negPeakTimes=NP_amplitudes;
        subplot(5,5,k)

heatmapArr=[negPeakTimes(arr_map_transp(1,1:2),sequenceNum)',nan,nan,nan,nan,ne
gPeakTimes(arr_map_transp(1,7:10),sequenceNum)';...

negPeakTimes(arr_map_transp(2,:),sequenceNum)';negPeakTimes(arr_map_transp(3,:)
,sequenceNum)';...

negPeakTimes(arr_map_transp(4,:),sequenceNum)';negPeakTimes(arr_map_transp(5,:)
,sequenceNum)';...
```

```
negPeakTimes(arr_map_transp(6,:),sequenceNum)';negPeakTimes(arr_map_transp(7,:)
,sequenceNum)';...

negPeakTimes(arr_map_transp(8,:),sequenceNum)';negPeakTimes(arr_map_transp(9,:)
,sequenceNum)';...
            negPeakTimes(arr_map_transp(10,:),sequenceNum)'];
        %         heatmapArr=interp2(heatmapArr,5);
        imagesc(heatmapArr), colormap("default"),colorbar % plot heatmap
    end
    h=h+25; % increment for subplot index
end

% save
("data","selected_spikes","peakIdx","peakVal","peaktime","IIS","data","gradVecx
","gradVecy","amplitude");
%% -------------------find amplitudes and indexes of all negative peaks on each
channel ------------------------
peakVal=negPeaks(:,selected_spikes);
peakIdx=negPeak_indexes(:,selected_spikes);
peaktime=time(negPeakLocs(:,selected_spikes));

%% ---------------plot spikes from a single channel-----------------
spikeNum=1:length(selected_spikes);
idx_inc=0;
% *********

figure;
```

```
for spikenum=1:100
    subplot(10,10,spikenum)

plot((1:6002)./30000,squeeze(IIS(28,spikenum,:)),"LineWidth",3,"Color","b");
%plot spike; 'squeeze' forces 3D into 2D
    hold on;
    plot(peakIdx(28,spikenum)./30000,peakVal(28,spikenum),'*',"LineWidth",3); %
    xlim([0 6002]./30000);xlabel('time(s)');ylabel("voltage(uV)")
end

%% ---------------creat 3D matrix container for all spikes------------
for i=1:96
    for j=1:length(selected_spikes)
        IIS(i,j,:)=windowPeaks.(field_names{i})(selected_spikes(j),:);
    end
end
figure,plot(squeeze(IIS(17,33,:))); % plot data from 3D array

% use 'squeeze' to squeeze 3D data into a 2D vector before plotting
%% creat multidimensional struct container for all spikes
for i=1:96
%     for j=1:length(selected_spikes)
        data(i).IIS=windowPeaks.(field_names{i})(selected_spikes,:);
%     end
end
figure,plot(data(23).IIS(19,:)); % plot data from struct
```

```
%% -------------plot spikes according to geometric layout of electrode grid----
------------
% electrode# to channel
chanloc=[1   2    nan nan nan nan 8    10   14   4;
         65  66   33  34  7    9    11   12   16   18;
         67  68   35  36  5    17   13   23   20   22;
         69  70   37  38  48   15   19   25   27   24;
         71  72   39  40  42   50   54   21   29   26;
         73  74   41  43  44   46   52   62   31   28;
         75  76   45  47  51   56   58   60   64   30;
         77  78   82  49  53   55   57   59   61   32;
         79  80   84  86  87   89   91   94   63   95;
         3   81   83  85  88   90   92   93   96   6];
    r=109:144;
    for c=1:2
        figure, plot_inc=0; spikenum=r(c);
        for idx1=1:10
            for idx2=1:10 % idx1 and idx2: for indexing into chanloc to make
plots according to geometric layout of array
                plot_idx=plot_inc+idx2; subplot(10,10,plot_idx)
                if ~isnan(chanloc(idx1,idx2))

plot(squeeze(IIS(chanloc(idx1,idx2),spikenum,:)),"LineWidth",1.3,"Color","b")
%plot spike
                    set(gca,'xtick',[]),set(gca,'ytick',[]) % remove
calibrations
                    grid on;
                    if chanloc(idx1,idx2)==1
```

```
                        title(['spike ' num2str(spikenum)]); % insert spike no.
as title of first plot
                    else
                        title(['channel ' num2str(chanloc(idx1,idx2))]); %add
channel number
                    end
                    hold on;
                    %plot location of negative peak

plot(peakIdx(chanloc(idx1,idx2),spikenum),peakVal(chanloc(idx1,idx2),spikenum),
'*',"LineWidth",1)
                    set(gca,'xtick',[])
                    hold on;   ylim([-3000 1000]);
                end
            end
            plot_inc=plot_inc+10;
        end
    end
%% ----------------------plot 2D heatmap of actual negative peak times (in
sec)--------------------------------
q=[2,8,14,16,19,21,26,31,33,44,48,52:54,72,80,88,93,75,109,113,125];
h=0;
for x=1:2
    figure
    for k=1:36
%         spikeNum=selected_spikes(k+h);
        spikeNum=116;
% figure
```

```
        avgMiddleFour=(peaktime(42,spikeNum)+peaktime(44,spikeNum)...
            +peaktime(46,spikeNum)+peaktime(50,spikeNum))./4;
        negPeakTimes=(peaktime-avgMiddleFour);
%         subplot(6,6,k)

heatmapArr=[negPeakTimes(chanloc(1,1:2),spikeNum)',nan,nan,nan,nan,negPeakTimes
(chanloc(1,7:10),spikeNum)';...

negPeakTimes(chanloc(2,:),spikeNum)';negPeakTimes(chanloc(3,:),spikeNum)';...

negPeakTimes(chanloc(4,:),spikeNum)';negPeakTimes(chanloc(5,:),spikeNum)';...

negPeakTimes(chanloc(6,:),spikeNum)';negPeakTimes(chanloc(7,:),spikeNum)';...

negPeakTimes(chanloc(8,:),spikeNum)';negPeakTimes(chanloc(9,:),spikeNum)';...
                    negPeakTimes(chanloc(10,:),spikeNum)'];
%         heatmapArr=interp2(heatmapArr,5);
        [Gx, Gy] = imgradientxy((heatmapArr),'central'); % calculate gradient
vectors
%         [Gmag, Gdir] = imgradient(Gx, Gy);
        title('spike '+string(spikeNum));
        imagesc(heatmapArr), colormap("default"),colorbar,hold on; % plot
heatmap
%
gradVecx(k)=mean(Gx,'all','omitnan');gradVecy(k)=mean(Gy,"all",'omitnan'); %
find mean of gradient vectors
          % each vector points in the direction of the greatest rate of
increase
```

```
        quiver(Gx,Gy,"Color","black","LineWidth",1.5,"ShowArrowHead","on"),hold
on;  %plot vector field;
    end
    h=h+36; % increment for subplot index
end

%% propagation direction

[Gmag,Gdir]=imgradient(gradVecx,gradVecy); % propagation speed (Gmag), and
direction

%----------polar plots----------%
% figure,compassHandle=compass(gradVecx,gradVecy),compassHandle.Color=[0 0 1];
% make compass plots using gradient vectors
[theta, r]=cart2pol(gradVecx,gradVecy); % convert gradient data points from
cartesian to polar
figure,polarhistogram(theta,"FaceColor","#4DBEEE","EdgeColor","b","LineWidth",1
.5)  % make polar histogram of all propagation directions
prop_dir_deg = rad2deg(theta);
colors_p = [linspace(0,1,200)', linspace(0,0,200)', linspace(1,0,200)']; % blue
to red colormap

figure % subplots of propagation speeds and directions
subplot(2,3,1),hold on,axis equal; % time aligned propagation directions
for k=1:length(gradVecy)
    compassHandle=compass(gradVecx(k),gradVecy(k));
    compassHandle.Color=colors_p(k,:);compassHandle.LineWidth=0.75;
end
```

```
subplot(2,3,2),compass(gradVecx,gradVecy); % propagation directions
% histogram of propagation directions
subplot(2,3,3),polarhistogram(theta,"FaceColor","#4DBEEE","EdgeColor","b","Line
Width",1.5);
subplot(2,3,[4:6]),figure,zz=zeros(size(Gmag)); % change of propagation speed
with time
figure,surface([1:200;1:200], [Gmag;Gmag], [zz;zz], [1:200;1:200],...
    'FaceColor', 'no',...
    'EdgeColor', 'interp',"LineWidth",1.5);colormap(colors_p);

figure,hold on,axis equal;
for k=1:length(gradVecy)
    compassHandle=compass(gradVecx(k),gradVecy(k));
    compassHandle.Color=colors_p(k,:);compassHandle.LineWidth=0.75;
%     compass(gradVecx(k),gradVecy(k));hold on;
    pause(0.2);
end

%-----------------plot 3D heatmap-----------------%

h=0;
for x=1:2
    figure
    for k=1:4
        spikeNum=k+h;
        avgMiddleFour=(peaktime(42,spikeNum)+peaktime(44,spikeNum)...
            +peaktime(46,spikeNum)+peaktime(50,spikeNum))./4;
        negPeakTimes=(peaktime-avgMiddleFour);
```

```
        subplot(2,2,k)

heatmapArr=[negPeakTimes(chanloc(1,1:2),spikeNum)',nan,nan,nan,nan,negPeakTimes
(chanloc(1,7:10),spikeNum)';...

negPeakTimes(chanloc(2,:),spikeNum)';negPeakTimes(chanloc(3,:),spikeNum)';...

negPeakTimes(chanloc(4,:),spikeNum)';negPeakTimes(chanloc(5,:),spikeNum)';...

negPeakTimes(chanloc(6,:),spikeNum)';negPeakTimes(chanloc(7,:),spikeNum)';...

negPeakTimes(chanloc(8,:),spikeNum)';negPeakTimes(chanloc(9,:),spikeNum)';...
            negPeakTimes(chanloc(10,:),spikeNum)'];
        heatmapArr=interp2(heatmapArr,5);
        [xx,yy]=meshgrid(1:length(heatmapArr),1:length(heatmapArr));
       surf(xx,yy,heatmapArr,"EdgeColor","none"), colormap("default")
        colorbar
    end
    h=h+4;
%     spikeidx=spikeNum;
end


%---------heatmap for amplitudes-----------%

h=0;
for x=1:12
    figure;
```

```
    for k=1:16
        spikeNum=k+h;
        subplot(4,4,k)
        amp_heat=-
[peakVal(chanloc(1,1:2),spikeNum)',nan,nan,nan,nan,peakVal(chanloc(1,7:10),spik
eNum)';...
            peakVal(chanloc(2,:),spikeNum)';peakVal(chanloc(3,:),spikeNum)';...
            peakVal(chanloc(4,:),spikeNum)';peakVal(chanloc(5,:),spikeNum)';...
            peakVal(chanloc(6,:),spikeNum)';peakVal(chanloc(7,:),spikeNum)';...
            peakVal(chanloc(8,:),spikeNum)';peakVal(chanloc(9,:),spikeNum)';...
            peakVal(chanloc(10,:),spikeNum)'];
        imagesc(amp_heat);colormap("default");
        colorbar;
    end
    h=h+16;
end

%-------------average amplitude heatmap----------------
avg_amp_mat = mean(peakVal,2); % calculate average amplitude matrix for all IIS
sequences
avg_sequence_amps = mean(peakVal); % calculate average amplitude for each IIS
sequence
% order average channel amplitudes according to geometric layout of MEA
amp_heatmap_avg = -
[avg_amp_mat(chanloc(1,1:2))',nan,nan,nan,nan,avg_amp_mat(chanloc(1,7:10))';...
            avg_amp_mat(chanloc(2,:))';avg_amp_mat(chanloc(3,:))';...
            avg_amp_mat(chanloc(4,:))';avg_amp_mat(chanloc(5,:))';...
            avg_amp_mat(chanloc(6,:))';avg_amp_mat(chanloc(7,:))';...
```

```
            avg_amp_mat(chanloc(8,:))';avg_amp_mat(chanloc(9,:))';...
            avg_amp_mat(chanloc(10,:))'];
% 3D plot of avg amplitudes according to geometric layout
[xx,yy]=meshgrid(1:length(amp_heatmap_avg),1:length(amp_heatmap_avg));
figure, subplot(2,2,1),imagesc(amp_heatmap_avg);colormap("default"),colorbar;
subplot(2,2,2),imagesc(interp2(amp_heatmap_avg,5));colormap("default"),colorbar
;
figure,histogram(avg_sequence_amps), title("Histogram of average interictal
spike amplitudes");
xlabel("Interictal spike amplitude (uV)"), ylabel("Interictal spike count");

figure,histogram(r), title("Histogram of interictal spike propagation speeds");
% plot interictal spike amplitudes
xlabel("Propagation speed"), ylabel("Interictal spike count");

figure,contourf(flipud(interp2(amp_heatmap_avg,5))),colormap(jet); % contour
map of avg amplitudes
%-----------3D plot of amplitude heatmap-----------------%

h=[159,112,74,77];
for x=1:2
    figure;
    for k=1:4
        spikeNum=74;
%         subplot(2,2,k)
        [xx,yy]=meshgrid(1:length( amplitude(spikeNum).heatmap),1:length(
amplitude(spikeNum).heatmap));
```

```
        surf(xx,yy, amplitude(spikeNum).heatmap,"EdgeColor","none"),
colormap(jet)
        colorbar
    end
    h=h+4;
end

%------------plot of IIS at early and late electrode-------(IIS time difference
plot)
sequenceNum = 181;
[first_IIS,a] = find(peaktime==min(peaktime(:,sequenceNum)));
[last_IIS,b] = find(peaktime==max(peaktime(:,sequenceNum)));
figure,plot((1:6002)./30000,squeeze(IIS([first_IIS,last_IIS],sequenceNum,:)),"L
ineWidth",1.5);
hold on;
plot(peakIdx([first_IIS,last_IIS],sequenceNum)./30000,peakVal([first_IIS,last_I
IS],sequenceNum),'*r',"LineWidth",1); %
xlim([0 6002]./30000);xlabel('time(s)');ylabel("voltage(uV)"); title(['IIS ',
num2str(sequenceNum)]);
legend(['electrode ',num2str(first_IIS)],['electrode ',num2str(last_IIS)]);
figure,histogram(prop_dir_deg), title("Histogram of propagation directions");
xlabel("Propagation direction (deg)"), ylabel("Interictal spike count");
figure,surface([1:200;1:200], [prop_dir_deg;prop_dir_deg], [zz;zz],
[1:200;1:200],...
    'FaceColor', 'no',...
    'EdgeColor', 'interp',"LineWidth",1);colormap(colors_p);
title("propagation direction over time"),xlabel("Interictal
spike"),ylabel("propagation direction(degreees)");
```

```
figure,plot(prop_dir_deg,"LineWidth",1);


figure,polarscatter(theta,r,[],1:200,"filled"),colormap(colors_p);
% stats for propagtion speed
mean_propagation_speed = mean(r); % mean propagation speed
max_propagation_speed = max(r); % max propagation speed
min_propagation_speed = min(r); % min propagation speeds
std_propagtion_speed = std(r); % standard deviation of propagation speeds

% stats for propagtion direction
mean_propagation_dir = mean(prop_dir_deg); % mean propagation direction
max_propagation_dir = max(prop_dir_deg); % max propagation dir
min_propagation_dir = min(prop_dir_deg); % min propagation dir
std_propagtion_dir = std(prop_dir_deg); % standard deviation of propagation
direction

% stats for average interictal spike amplitude
mean_avg_sequence_amps = mean(avg_sequence_amps); % mean of average interictal
spike amplitudes
max_avg_sequence_amps = max(avg_sequence_amps); % max of average interictal
spike amplitudes
min_avg_sequence_amps = min(avg_sequence_amps); % min of average interictal
spike amplitudes
std_avg_sequence_amps = std(avg_sequence_amps); % standard deviation of average
interictal spike amplitudes
```